LITHOS 434-435 (2022) 106937

Contents lists available at ScienceDirect

LITHOS

journal homepage: www.elsevier.com/locate/lithos

The earliest stage of mantle-melt evolution during subduction initiation: Evidence from the Neo-Tethyan Mirdita Ophiolite, Albania

Weiwei Wu [a,b,*], Jingsui Yang [a,b,*], Jianping Zheng [c], Dongyang Lian [a,b], Ibrahim Milushi [d], Yu Yang [a], Tian Qiu [b], Huichao Rui [c], Guolin Guo [e], Zhihui Dai [f], Ahmed Elsaid Ismail Masoud [g]

[a] State Key Laboratory for Mineral Deposits Research, School of Earth Sciences and Engineering, Nanjing University, Nanjing 210023, China
[b] Center for Advanced Research on Mantle (CARMA), Key Laboratory of Deep-Earth Dynamics of Ministry of Natural Resources, Institute of Geology, Chinese Academy of Geological Sciences, Beijing 100037, China
[c] School of Earth Sciences, China University of Geosciences, Wuhan 430074, China
[d] Institute of Geosciences, Energy, Water and Environment, Polytechnic University of Tirana, Rruga: Don Bosko nr. 60, Tirana 1000, Albania
[e] State Key Laboratory of Nuclear Resources and Environment, East China University of Technology, Nanchang 330013, Jiangxi, China
[f] Institute of geochemistry, Chinese Academy of Sciences, Guiyang 550081, China
[g] Geology Department, Faculty of Science, Tanta University, Tanta 31527, Egypt

ARTICLE INFO

Keywords:
Subduction initiation
Mantle-melt evolution
Mirdita ophiolite
Albania

ABSTRACT

Mantle-melt evolution processes in the earliest stage of subduction initiation (SI) are still ambiguous. Here, we report the systematic petrogeochemical and physical records of the SI processes demonstrated by the Gomsiqe massif, Mirdita ophiolite. The Gomsiqe ultramafic body consists of basal lherzolites, upper harzburgites containing lentoid dunites and disseminated chromitites, displaying transition of petrological (Cr# of spinels range from 12.7 to 47.1) and geochemical signatures. Clinopyroxene trace element modeling indicates that lherzolites and harzburgites have undergone variable garnet-facies melting prior to spinel-facies melting. Harzburgites encountered higher degrees of spinel-facies melting compared with those of lherzolites (~ 8–10% vs. ~ 3–5%), and late-stage MORB melt metasomatism. Lherzolites escaped metasomatism. The dunites and chromitites formed by interactions between the harzburgitic lithosphere and MORB-like transitional magmas continued, but with limited hydrous fluid involvement during subduction. The transitional characteristics of metasomatic melt composition and physical condition (i.e., oxygen fugacity [fo_2]) of different lithologies are consistent with the corresponding archive in the Izu-Bonin-Mariana forearc. Lherzolites and harzburgites have comparable fo_2 to that of the abyssal peridotites. The dunites are apparently more oxidized compared to the associated chromitites, further supporting a hypothesis that sulfur-saturated MORB melts were responsible for the formation of chromitites and reduced Cr# of chromitite spinels. Thermometry showed that lherzolites preserved higher equilibration temperatures than harzburgites. Both experienced a later lower-temperature re-equilibration process. Thus, the Mirdita ophiolite preserves multi-stage mantle-melt evolution processes, which are the comprehensive physicochemical responses of the earliest stage of SI.

1. Introduction

Subduction initiation (SI) process is essential for a comprehensive understanding of the origin of plate tectonics (Reagan et al., 2010; Stern et al., 2013; Ishizuka et al., 2014; Whattam and Stern, 2011). However, modern forearcs related to oceanic subduction initiation process are distant from continents and mostly lie in the deep trenches. Except for a few active examples (e.g., the Izu-Bonin-Mariana (IBM) arc and Vanuatu-Tonga arc) sampled via drilling, diving and dredging (Reagan et al., 2010; Stern et al., 2013), the lithosphere of many intra-oceanic forearcs is remarkably misty, but preserves a high-fidelity petrological record of SI. The "subduction initiation rule" (SIR) (Whattam and Stern, 2011) proposes that the magmatic sequence preserved in ophiolite and modern forearc volcanic sections follow a predictable chemotemporal and/or chemostratigraphic vertical progression. In comparison with modern forearcs, SIR ophiolites (Whattam and Stern, 2011) are relics of ancient intra-oceanic forearc lithosphere thrust onto continents (Dilek, 2003; Shervais, 2001) and are therefore accessible for comprehensive

* Corresponding authors at: 163 Xianlin Road, Qixia District, Nanjing, Jiangsu Province 210023, China.
E-mail addresses: cugcags@163.com (W. Wu), yangjsui@163.com (J. Yang).

https://doi.org/10.1016/j.lithos.2022.106937
Received 6 June 2022; Received in revised form 18 September 2022; Accepted 30 October 2022
Available online 4 November 2022

research. Although extensive studies have been conducted on extrusive rocks in the IBM forearc and SIR ophiolites (Dilek et al., 2008; Ishizuka et al., 2014; Reagan et al., 2010; Stern et al., 2013; Whattam and Stern, 2011), the complementary mantle-melt evolutionary process preserved in peridotites related to magmatic activity corresponding to changes in tectonic settings in the earliest stages of subduction initiation is still ambiguous. Thus, use of SIR ophiolitic peridotites can accelerate and complete our understanding of geodynamic processes associated with subduction initiation (Stern et al., 2013).

Early studies distinguished two types of ophiolites in northern Albania, the western (WMO) and eastern Mirdita ophiolite (EMO), according to their distinct lithological units and petrology and geochemistry characteristics (Dilek et al., 2008; Hoeck et al., 2002; Saccani et al., 2018 and references therein). WMO predominantly has a mid-ocean ridge (MOR) signature, while the EMO demonstrates a supra-subduction zone (SSZ) signature (Dilek et al., 2008; Hoeck et al.,

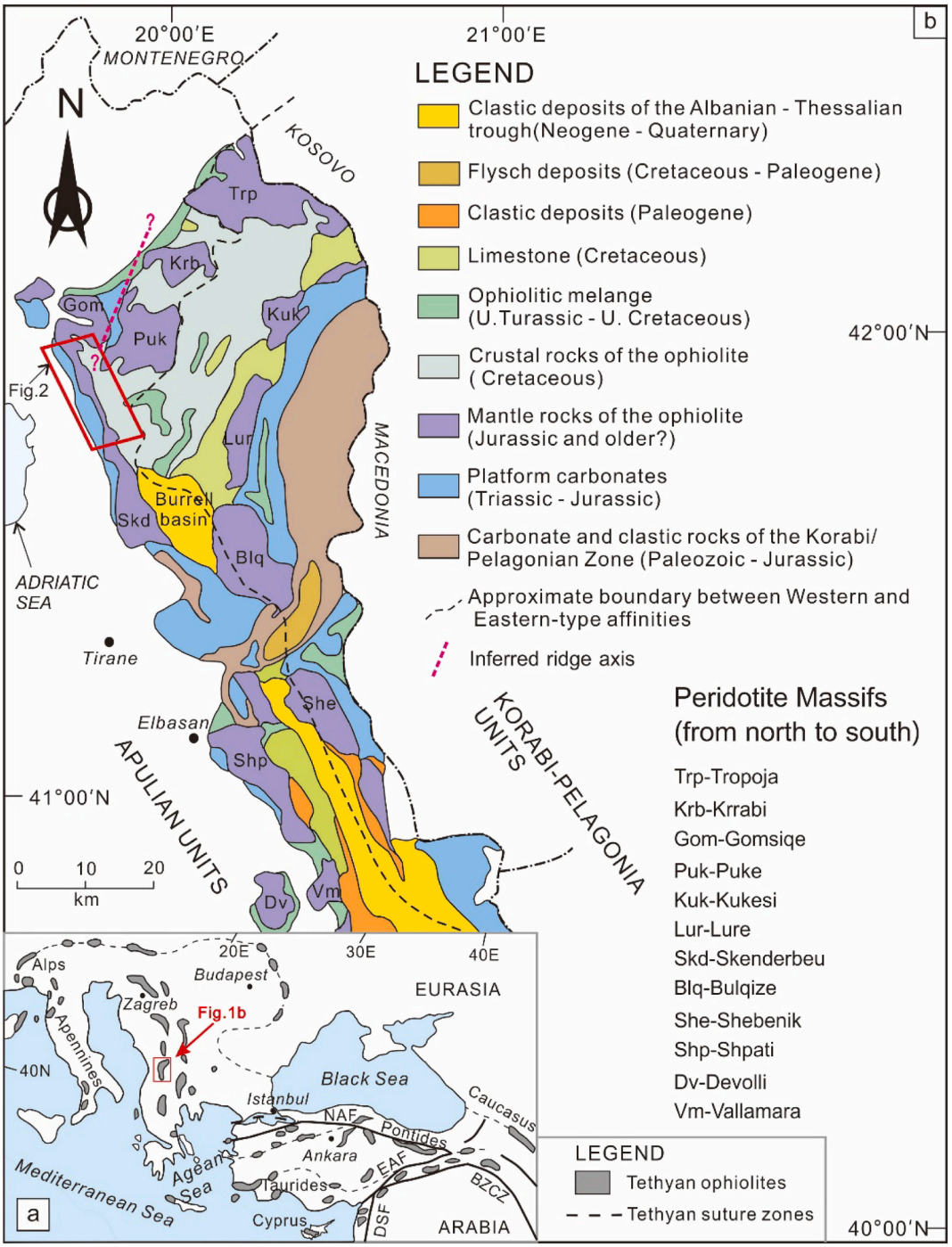

Fig. 1. Locations of Tethyan ophiolites in the Mediterranean (a), and major peridotite massifs in the Mirdita ophiolites, northern Albania (b) (modified from Wu et al., 2018). Abbreviations in Fig. 1a: BZCZ-Bitlis Zagros Collision Zone, DSF-Dead Sea Fault, EAF-East Anatolian Fault, NAF-North Anatolian Fault. Red dashed line in Fig. 1b represents the inferred ridge axes suggested by Nicolas et al. (1999). (For interpretation of the references to colour in this figure legend, the reader is referred to the web version of this article.)

2002). To date, the coexistence of MOR-type and SSZ-type ophiolites in Albania has been explained by subduction initiated near a mid-ocean ridge (Hoeck et al., 2002), westward-dipping intra-oceanic subduction associated with subsequent rapid slab rollback (Dilek et al., 2008), and some variants of the two (Saccani et al., 2018; Wu et al., 2018). Constraints obtained from the spatial-temporal relationships of the extrusive crustal rocks in the ophiolites indicate that a forearc tectonic setting followed by a SIR origin is responsible for the formation of the Mirdita ophiolites (Saccani et al., 2018). A similar evolutionary history has been discovered in the IBM forearc (Ishizuka et al., 2014; Pearce et al., 1992; Reagan et al., 2010), Troodos (Pearce et al., 1984), Semail (Alabaster et al., 1982), and other SSZ ophiolites worldwide (Dilek, 2003).

The Gomsiqe massif belongs to the WMO, and is located near the inferred ridge axis (Nicolas et al., 1999) and tentative geochemical boundary between the WMO and EMO (Fig. 1). Here, we provide new comprehensive petrographic, mineralogical, geochemical, and thermal estimation evidence obtained from the Gomsiqe mantle peridotites (basal lherzolite, harzburgite, and dunite) and associated disseminated chromitites (high-Al type). The findings of this study aid in understanding the mantle-melt evolution processes of the Gomsiqe ultramafic body, which is corresponding to changes in tectonic settings in the earliest stage of subduction initiation, the physical conditions, and the mechanism of podiform chromitite genesis.

2. Geological framework and petrology

Mesozoic ophiolites that occur in the Mediterranean are remnants of oceanic lithosphere developed in different spreading centers in the Neo-Tethyan Ocean, which separated a succession of Gondwana-related continental blocks (Fig. 1a) (Dilek et al., 2008; Saccani et al., 2018). The Jurassic (165–160 Ma) Mirdita ophiolite zone (northern Albania) extends approximately NW-SE, and is approximately 30 km wide with Apulian units in the west and the Korabi-Pelagonia units in the east (Fig. 1b) (Dilek et al., 2008). It was suggested to have formed at a slow-spreading ridge based on regional structural mapping (Nicolas et al., 1999). Constraints obtained from paleomagnetism studies of the sheeted dykes of the Mirdita ophiolite and paleogeography obtained from plate kinematic reconstructions indicate that the ridge axis located between the Gomsiqe and Puka massif has a N-S to NNE-SSW orientation (Fig. 1; Nicolas et al., 1999; Maffione et al., 2015). Mirdita ophiolite escaped

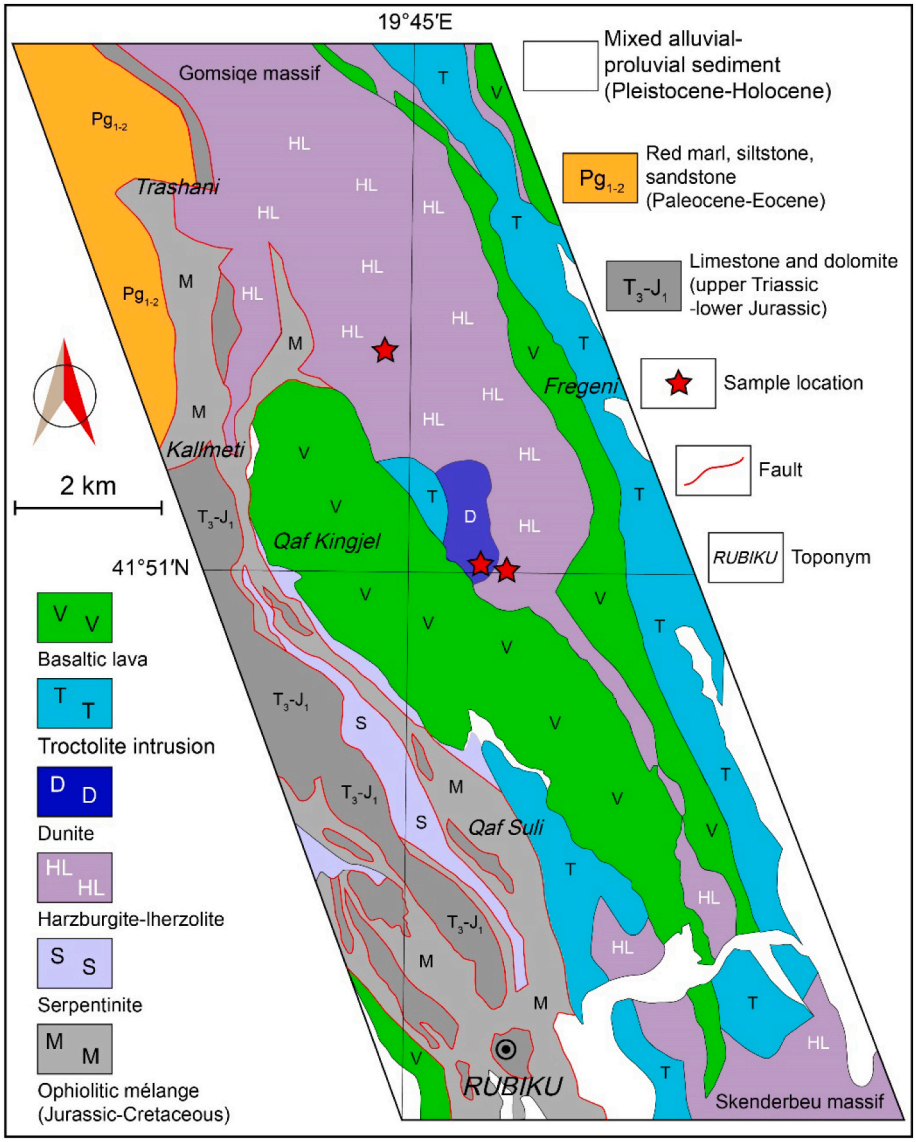

Fig. 2. Simplified geological map of the Gomsiqe massif, western Mirdita ophiolite (after Xhomo et al., 2002).

most Alpine and Cenozoic tectonic events due to its >15 km-thick ophiolitic basement (Nicolas et al., 1999). Consequently, it preserves a complete ophiolite rock, of which the structural, chemo-stratigraphy, and geochemical characteristics of the crustal volcanic rocks have been widely studied (Dilek, 2003; Dilek et al., 2008; Hoeck et al., 2002; Saccani et al., 2018). In recent years, microdiamonds and other ultrahigh-pressure minerals have been discovered in the peridotites and chromitites from Mirdita ophiolite (Wu et al., 2019; Xiong et al., 2017a), which indicate a deep mantle origin. The findings suggest that more in-depth research is needed for the Mirdita mantle rocks.

The mantle rocks of the Gomsiqe massif are composed of, from the bottom (westward) to the top (eastward), lherzolites, harzburgites with lentoid dunite, and sparse podiform chromitites (Fig. 2). Foliated lherzolites are situated at the basal part of the mantle sequence (Figs. 2 and 3), consistent with the occurrence of basal lherzolite in the Wadi Sarami, central Oman ophiolite (Khedr et al., 2014), whereas foliated harzburgite and dunite (including high-Al podiform chromitite) (Fig. 3) are predominantly observed at shallow mantle depths. See Appendix A[1] for full sample description.

3. Sample preparation and analytical methods

We chose to collect relatively fresh mantle samples from the Gomsiqe massif, including basal lherzolites, harzburgites, lentoid dunites, and integrated disseminated chromitite (Figs. 3, 4). The sample locations are shown in Fig. 2. Mineral (olivine (Ol), orthopyroxene (Opx), clinopyroxene (Cpx), spinel (Spl), and pargasite (Prg)) chemistry analyses were performed with an electron microprobe (JEOL JXA-8100) at the Chinese Academy of Geological Sciences, the Second Institute of Oceanography, MNR (JEOL JXA-8100), and the East China University of Technology (JEOL JXA-8230). More analytical details can be found in Wu et al. (2018). Trace element analysis of minerals (Ol, Opx, Cpx, and Spl) was conducted at the Chinese Academy of Sciences (Guiyang) using LA-ICP-MS. Trace element concentrations of Ol, Opx, Cpx and Spl were determined by a GeoLasPro laser-ablation system (Lamda Physik, Gottingen, Germany) coupled to an Agilent 7700× ICP-MS. Each analysis was performed by ablating 40 μm diameter spots at 6 Hz with energy of ~100 mJ per pulse for 45 s after measuring the gas blank for 20 s. The standard reference materials SRM610, SRM612, CGSG-1, CGSG-2, BHVO-2G, BCR-2G and BIR-1G were used as external standards, together with Al as internal standard elements for Spl, to plot calibration curves. Every fifteen analysis was followed by five analysis of reference materials to monitor the time-dependent calibration for sensitivity drift. Whole-rock major and trace elements were obtained from the Wuhan SampleSolution Analytical Technology Co., Ltd., China and the National Research Center for Geoanalysis (Beijing). Detailed analytical processes are described in Wu et al. (2018).

4. Mineral and whole-rock chemistry

4.1. Mineral major oxide compositions

4.1.1. Olivine (Ol)

All olivines are highly magnesian (Fo > 89.7; Supplementary Table A1[2]); however, they show significant differences among the different lithologies. Generally, the granular olivines in basal lherzolites have Fo contents of 89.7–90.4, and NiO contents of 0.34–0.43 wt%, which are similar to those of Oman Semail basal lherzolites (Fig. 5; Khedr et al., 2014). Olivines in harzburgites are characterized by similar or slightly higher Fo and NiO contents than those of the olivine grains in the Gomsiqe lherzolites (Fig. 5). Olivine in dunites has Fo contents of 90.2–92.2 (average of 91.2) and NiO contents of 0.22–0.43 wt%

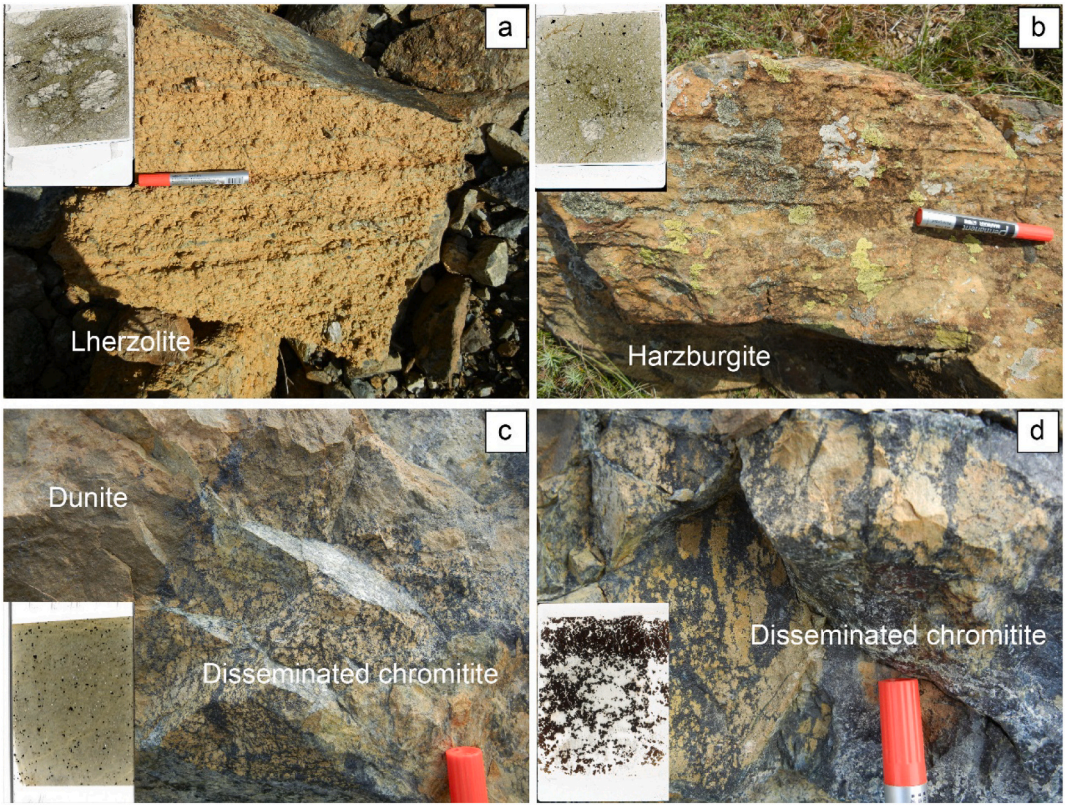

Fig. 3. Field photographs of the Gomsiqe massif, western Mirdita ophiolite. (a) Fresh mantle basal lherzolite having lineation of mineral pyroxenes; (b) Fresh mantle harzburgite having lineation of mineral pyroxenes; (c) Disseminated chromitites hosted by dunite envelop; (d) Disseminated chromitite.

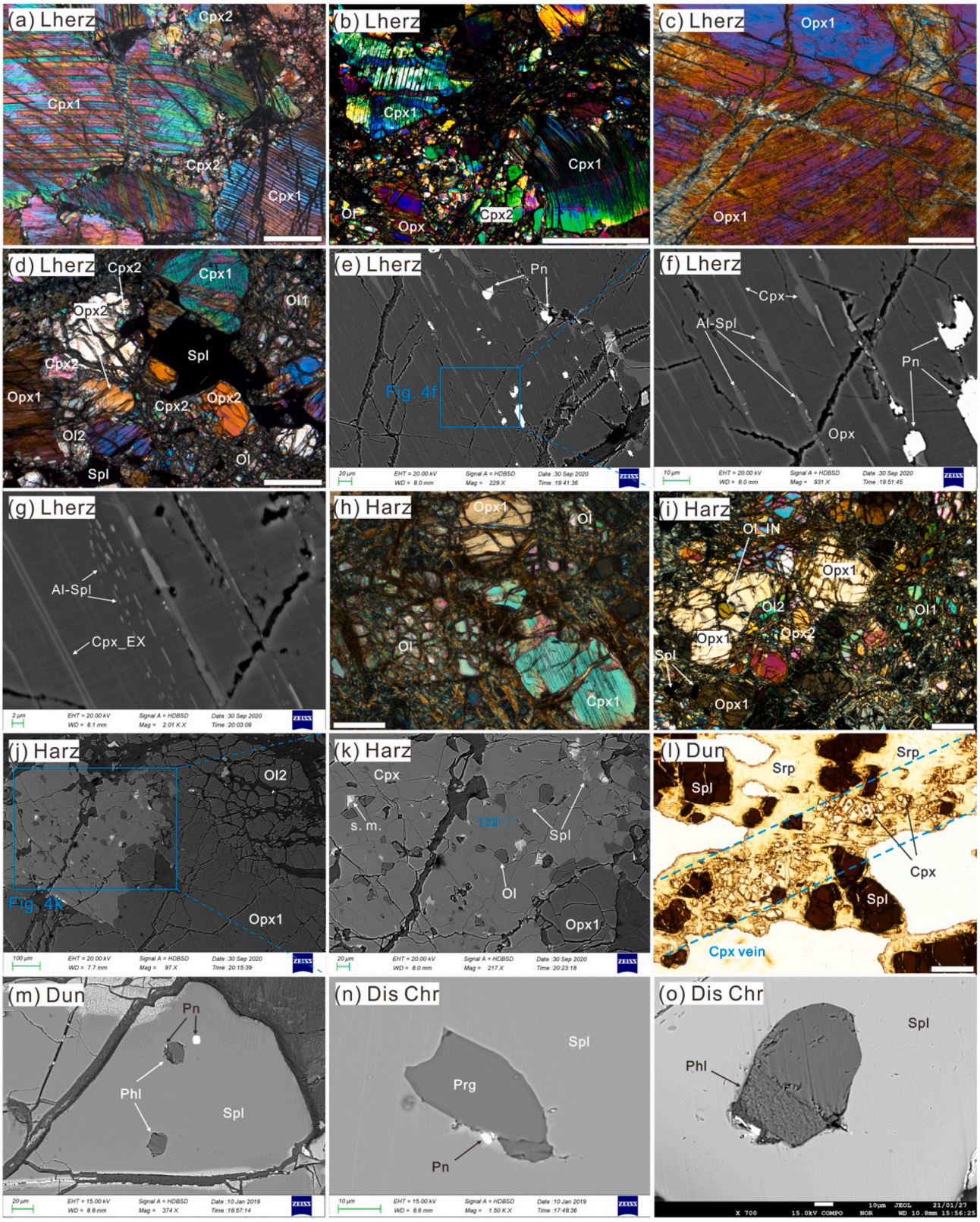

(caption on next page)

Fig. 4. Photomicrographs of representative basal lherzolites (a-g), harzburgites (h-k), dunites (l-m) and disseminated chromitites (n-o) from the Gomsiqe massif. (a) Lherzolite (cross-polarized light), porphyroclastic and granular texture. Laminated fine-grained Cpxs (subhedral) occur as grain aggregates or patchy, indicating primitive feature, and contrasting with anhedral interstitial Cpxs; (b) Lherzolite (cross-polarized light), porphyroclastic and granular texture. Cpx porphyroclasts develop undulatory extinction, and occasionally form fine Cpx2 minerals in the matrix; (c) Lherzolite (cross-polarized light), porphyroblastic and granular texture. Opx1 porphyroclasts show plastic deformation; (d) Lherzolite (cross-polarized light), granular texture. Intergrowth of Ol2 + Opx2 + Cpx2 + Spl; (e) - (g) Lherzolite (black scattered electron image, BSE). Coarse Opx porphyroclasts contain Cpx + Spl lamellae and sulfides inclusions (mainly pentlandite, and pyrrhotite); (h) and (i) Harzburgite (cross-polarized light), porphyroclastic and granular texture. The porphyroclastic Opx is enclosed by a matrix assembly of Ol2 + Cpx2 + Opx2 + Spl, with exsolution lamellae of Cpx (Cpx_EX) and inclusions of Ol (Ol_IN); (j) and (k) Harzburgite (BSE). The porphyroclastic Opx1 shows reaction margin consist of fine mineral assemblies of Cpx2 + Ol2 + Spl ± Opx2 ± serpentine ± sulfide; (l) Dunite (plane-polarized light), granular texture. Note the veinlet texture of clinopyroxenes; (m) Dunite (BSE). Phlogopite (Phl) and pentlandite (Pn) inclusions hosted in the chromium spinels; (n) Disseminated chromitite (BSE). Pargasite (Prg) and pentlandite (Pn) inclusions hosted in the chromium spinels; (o) Disseminated chromitite (BSE). Phlogopite (Phl) inclusions hosted in the chromium spinels. Abbreviations: Lherz-lherzolite, Harz-harzburgite, Dun-dunite, Dis Chr-disseminated chromitite, Srp-serpentine, Phl-phlogopite, Prg-pargasite, Pn-pentlandite, s.m.-secondary mineral. White lines in (a-d), (h-i) and (l) are 500 μm in length.

(average of 0.33 wt%) (Table A1; Fig. 5). In detail, dunite proximal to disseminated chromitites (i.e., samples 16AS160 and 16AS162, hereafter termed as Du-prox.), has higher Fo contents (average of 91.9 vs. 90.5, respectively) of Ol grains than those of Ol grains in the dunites distal to disseminated chromitites (termed as Du-distal; i.e., sample 16AS158). The range of Fo values of the Gomsiqe peridotites and NiO contents are comparable with those of olivines from global abyssal peridotites (Fig. 5). As to the disseminated chromitites, olivines have the highest Fo values of 92.6–92.9 and NiO contents of 0.34–0.51 wt%, compared with those of other Gomsiqe lithologies.

4.1.2. Orthopyroxene (Opx)

Representative microprobe analyses of Opx are shown in Table A2. Opx mainly occur in the lherzolites and harzburgites. Porphyroclastic Opxs (i.e., Opx1) in the Gomsiqe basal lherzolites show higher contents of Al_2O_3 than those of porphyroclastic Opx in harzburgites (Fig. 5b). In both peridotites, Opx2 (e.g., fine-grained orthopyroxenes around porphyroclastic Opx/Cpx) commonly shows lower contents of Al_2O_3, but slightly higher Mg# than Opx1 (Fig. 5b). In the plot of Mg# versus Al_2O_3 (Fig. 5b), Opx1 in Gomsiqe lherzolites is similar to global abyssal lherzolites (Warren, 2016) and the Wadi Sarami Type 2 lherzolites, Oman ophiolite (Khedr et al., 2014), while the Opx1 in the Gomsiqe harzburgites is comparable to Opx in global abyssal harzburgites (Warren, 2016) and the Wadi Sarami Type 1 lherzolite, Oman ophiolite (Khedr et al., 2014).

4.1.3. Clinopyroxene (Cpx)

Clinopyroxenes occur in basal lherzolites, harzburgites, and dunites, all of which are diopside (Table A3). In detail, Cpxs in the lherzolites exhibit higher contents of Al_2O_3 (Fig. 5c), Na_2O (Fig. 5d), and TiO_2, similar Cr_2O_3 (Fig. 5e), but lower Mg# (Fig. 5c–d), than Cpx within the Gomsiqe harzburgites. Additionally, Cpx2 (e.g., fine-grained clinopyroxenes around porphyroclastic Opx/Cpx) grains in both peridotite types, have lower Al_2O_3 (Fig. 5c), Na_2O (Fig. 5d), and Cr_2O_3 (Fig. 5e), but slightly higher Mg# (Fig. 5c–d), than those of Cpx1 (e.g., coarse-grained porphyroclastic clinopyroxene). Exsolved Cpx (termed as Cpx_EX) within the Opx porphyroclasts, in both peridotites, have the highest Al_2O_3 and Cr_2O_3 contents, but similar or slightly lower Mg# values compared with those of other types of Cpx (i.e., Cpx1 and Cpx2) (Fig. 5c–e). In general, Cpx in lherzolites are more similar to those of global abyssal lherzolites (Warren, 2016), and Wadi Sarami Type 2 lherzolite, Oman ophiolite (Khedr et al., 2014), the latter of which formed during the early stage of subduction initiation. Additionally, Cpx in harzburgites are similar to those of Cpx in global abyssal harzburgites (Warren, 2016) and Wadi Sarami Type 1 lherzolites, Oman ophiolite (Khedr et al., 2014).

Cpx grains in Gomsiqe Du-distal have lower contents of Al_2O_3 (Fig. 5c), Na_2O (Fig. 5d), and similar Mg#, compared to those of Cpx in the Gomsiqe Du-prox. Clinopyroxene inclusions (Cpx_IN) in Du-prox. show larger variation range of Cr_2O_3 contents relative to other types of Cpx within dunites at similar Al_2O_3 contents (Fig. 5e).

4.1.4. Spinel (Spl)

The composition of Spl from the Gomsiqe peridotites and chromitites shows a wide compositional range in terms of Cr# (100*Cr/(Cr + Al)) (Arai, 1994). All of the spinels belonged to the high-Al type (Cr# < 60; Arai, 1994) (Table A4). Spl minerals in the Gomsiqe lherzolites exhibit higher contents of Al_2O_3 (53.1–55.8 wt% vs. 28.6–32.8 wt%) and Mg# (72.4–74.4 vs. 52.6–54.5), but lower TiO_2 (0.01–0.12 wt% vs. 0.08–0.21 wt%) and Cr# (12.7–16.1 vs. 40.5–47.1), than those in the harzburgites (Fig. 6). The Gomsiqe lherzolitic spinel compositions are similar to lherzolitic spinels formed in mid-ocean ridges (Warren, 2016) and central Oman ophiolite (Khedr et al., 2014), while the Gomsiqe harzburgitic spinel compositions are akin to those of abyssal harzburgites (Warren, 2016) and Oman harzburgites (Hanghøj et al., 2010; Takazawa et al., 2003).

In the dunites and disseminated chromitites, the Spl grains show higher contents of Al_2O_3, TiO_2, and Mg#, and lower Cr#, than those of the Gomsiqe harzburgites (Fig. 6). Their compositions are consistent with those of typical high-Al type chromitites (Zhou et al., 2014), spinels crystallized from MORB (Barnes and Roeder, 2001), and chromitites found in modern mid-ocean ridges (Abe, 2011; Arai and Matsukage, 1998; Morishita et al., 2007); however, they are quite different from those of boninites (Barnes and Roeder, 2001), and the peridotitic spinel formed in the forearc (Fig. 6c and d).

4.1.5. Pargasite (Prg)

Pargasites are only found as inclusions within chromium spinel in the Gomsiqe dunites and disseminated chromitites (Fig. 4, Table A5). Prg inclusions in spinels within Du-prox. have higher Al_2O_3 contents (13.0–14.8 wt% vs. 13.3–14.2 wt%), similar Na_2O (2.91–3.84 wt% vs. 3.11–3.71 wt%), and lower TiO_2 contents (0.58–0.99 wt% vs. 0.88–1.15 wt%), compared with those of disseminated chromitites (Fig. 5f). Pargasites in Du-distal show the lowest TiO_2 content compared to Du-prox. and disseminated chromitites. Compared to pargasite inclusions formed in typical mid-oceanic ridge dunites (Morishita et al., 2011), those in Gomsiqe dunites and chromitites have similar Na_2O, but lower TiO_2 (Fig. 5f). However, the Gomsiqe Prgs show higher TiO_2 contents than those in IBM medium-Cr# dunite, which formed by interaction with a MORB-like forearc basalt (FAB) (Morishita et al., 2011).

4.2. Mineral trace-element compositions

4.2.1. Olivine (Ol)

Representative trace element compositions of Ol from the Gomsiqe peridotites are shown in Table A7. Cr# of olivines are strongly correlated with those of spinels from Gomsiqe peridotites, as well as all peridotite types (Fig. A1a) (De Hoog et al., 2010). Olivines from basal lherzolites and harzburgites in Gomsiqe have relatively high Ni (3050–3090 ppm vs. 2972–3136 ppm), lower Mn (963–1033 ppm vs. 1132–1206 ppm) and similar Co (140–147 ppm vs. 137–148 ppm) concentrations, along with the relatively low Fo (89.5–90.1 vs. 89.5–90.3) (Fig. 7, Fig. A1). Olivine in the Gomsiqe lherzolites have lower Mn concentrations than those in the harzburgites (Fig. 7a). In the

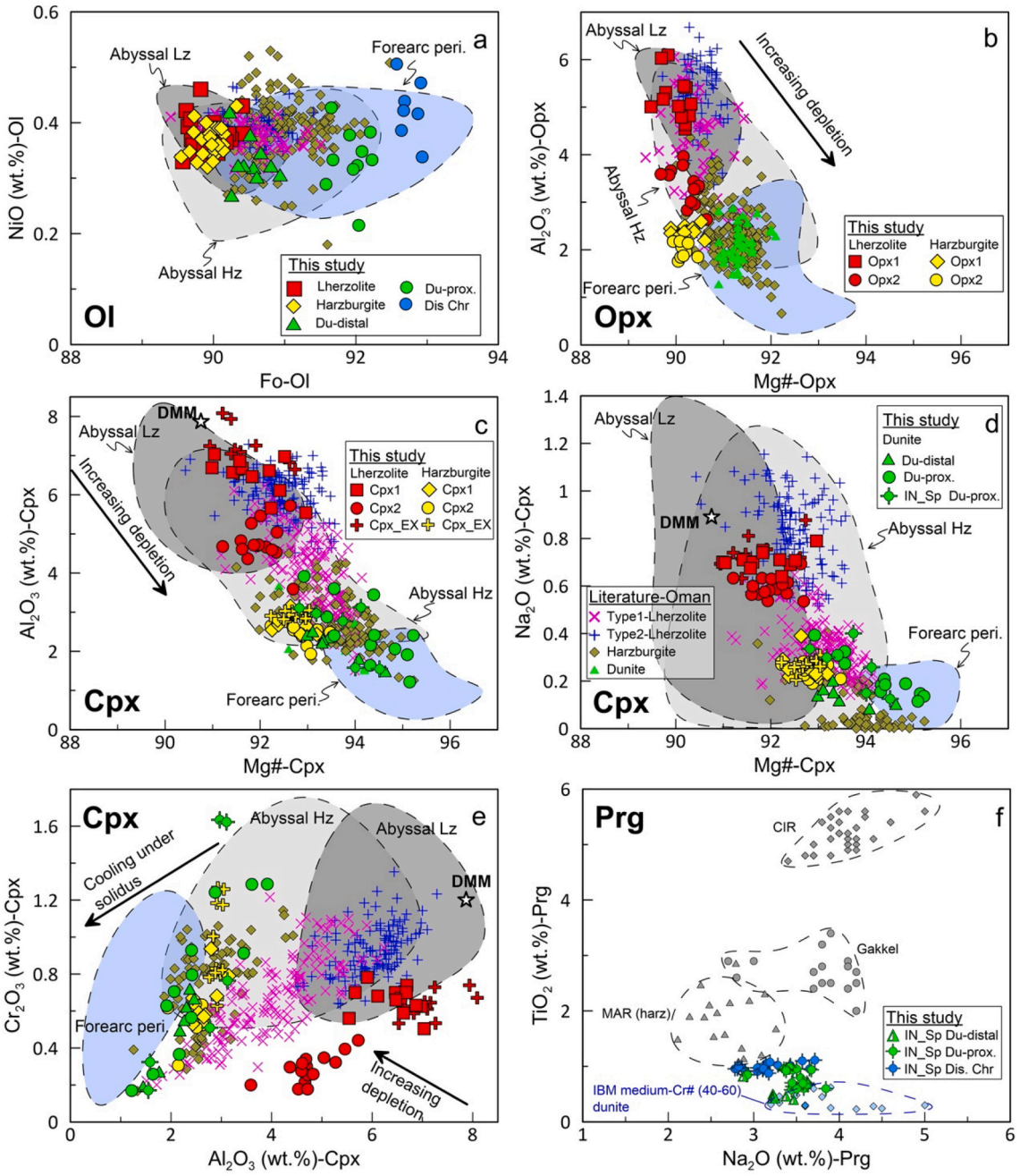

Fig. 5. Mineral compositional variations from the Gomsiqe massif, Mirdita ophiolite. Ol: Fo vs. NiO (wt%) (a); Opx: Mg# vs. Al_2O_3 (wt%) (b); Cpx: Mg# vs. Al_2O_3 (wt%) (c), Na_2O (wt%) (d), and Al_2O_3 (wt%) vs. Cr_2O_3 (wt%) (e); Prg: Na_2O (wt%) vs. TiO_2 (wt%) (f). Abyssal lherzolite (Abyssal Lz) and abyssal harzburgite (Abyssal Hz) fields are from Warren (2016) and references therein. Forearc peridotites (Forearc peri.) field is from Ishii et al. (1992), Parkinson and Pearce (1998), and Okamura et al. (2006). Data for Oman ophiolites are from Takazawa et al. (2003), Hanghøj et al. (2010), and Khedr et al. (2014). Data for pargasite inclusions within spinels from Izu-Bonin-Mariana and mid-oceanic ridge systems are provided by Morishita et al. (2011). Depleted MORB mantle (DMM) is shown here for comparison (Workman and Hart, 2005). Abbreviations: CIR-Central Indian Ridge, MAR-Mid-Atlantic Ridge, Gakkel-Gakkel Ridge, IBM-Izu-Bonin-Mariana.

dunites and disseminated chromitites, olivines have lower Ni and Mn concentrations than olivine in the Gomsiqe harzburgites (Fig. 7). Additionally, olivines from dunites show similar Ni, Mn, and Co concentrations to those in replacive dunites (Lanzo South massif; Sanfilippo et al., 2014) and Purang dunites (Su et al., 2019) (Fig. 7, Fig. A1c).

4.2.2. Clinopyroxene (Cpx)

Overall, Cpx from different Gomsiqe peridotites show similar chondrite-normalized REE patterns, with relatively flat middle-heavy rare earth element (M-HREE) patterns, and depletion in light rare earth elements (LREE) (Fig. 8a; Table A8). The HREE patterns of the Gomsiqe lherzolitic Cpx are compatible with those of Cpx from DMM (Fig. 8a), whereas the L-MREE abundances are evidently lower than those of Cpx from DMM (Workman and Hart, 2005). The REE patterns of the lherzolitic and harzburgitic Cpx are similar to those of Cpx in abyssal lherzolites and harzburgites, respectively (Fig. 8a). Gomsiqe lherzolitic Cpxs have chondrite-normalized REE patterns that are similar to those of Oman lherzolitic Cpx (Fig. 8c), especially the type 2 lherzolitic Cpx (Khedr et al., 2014). Additionally, dunitic Cpx have noticeably lower absolute abundances of M-HREE (Fig. 8) and higher $(LREE/MREE)_N$ ratios than those of harzburgites and lherzolites. In PM-normalized trace-element spider diagrams (Fig. 8b), Cpx in lherzolites and

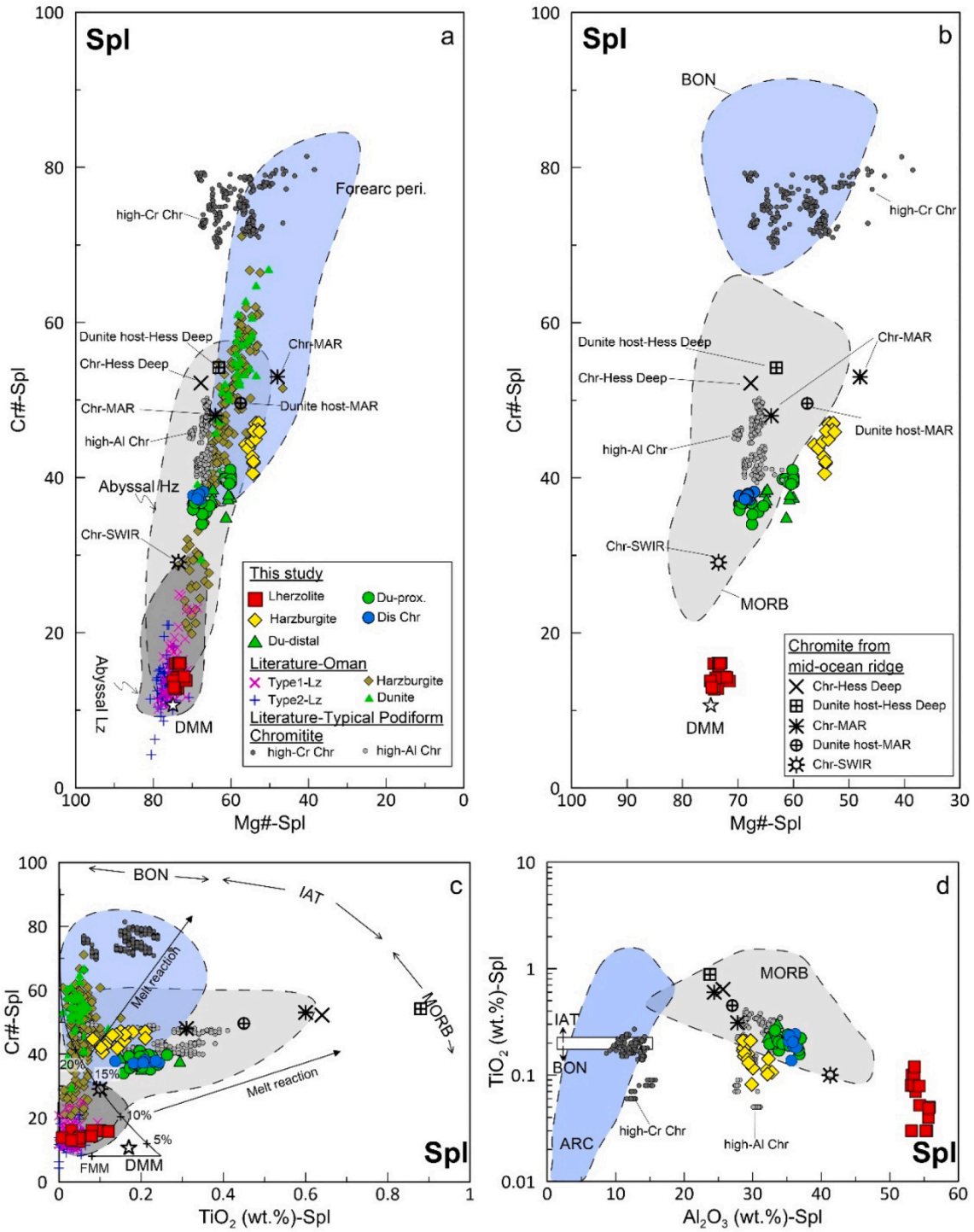

Fig. 6. Variations of Mg# vs. Cr# (a, b), TiO_2 (wt%) vs. Cr# (c), and Al_2O_3 (wt%) vs. TiO_2 (wt%) (d) of spinel from the Gomsiqe massif, Mirdita ophiolite. In Fig. 6b, the compositions of chromium spinel from boninite (BON) and MORB, respectively, are from Barnes and Roeder (2001). In Fig. 6d, the compositional variations of chromium spinel from MORB and arc-related volcanic rocks (ARC), respectively, are from Kamenetsky et al. (2001), and the white rectangle represents the transition of spinel TiO_2 contents between island-arc basalt (IAB) and BON. Data for abyssal peridotites, forearc peridotites, and Oman ophiolite are from the same references used in Fig. 5. Data for typical podiform chromitites are from Zhou et al. (2014). Data of Spl from modern mid-oceanic ridge systems are provided by Arai and Matsukage (1998) (Hess Deep), Morishita et al. (2007) (SWIR, Southwest Indian Ridge), and Abe (2011) (MAR, Mid-Atlantic Ridge). Data of Spl from the depleted MORB mantle (DMM) is given by Workman and Hart (2005).

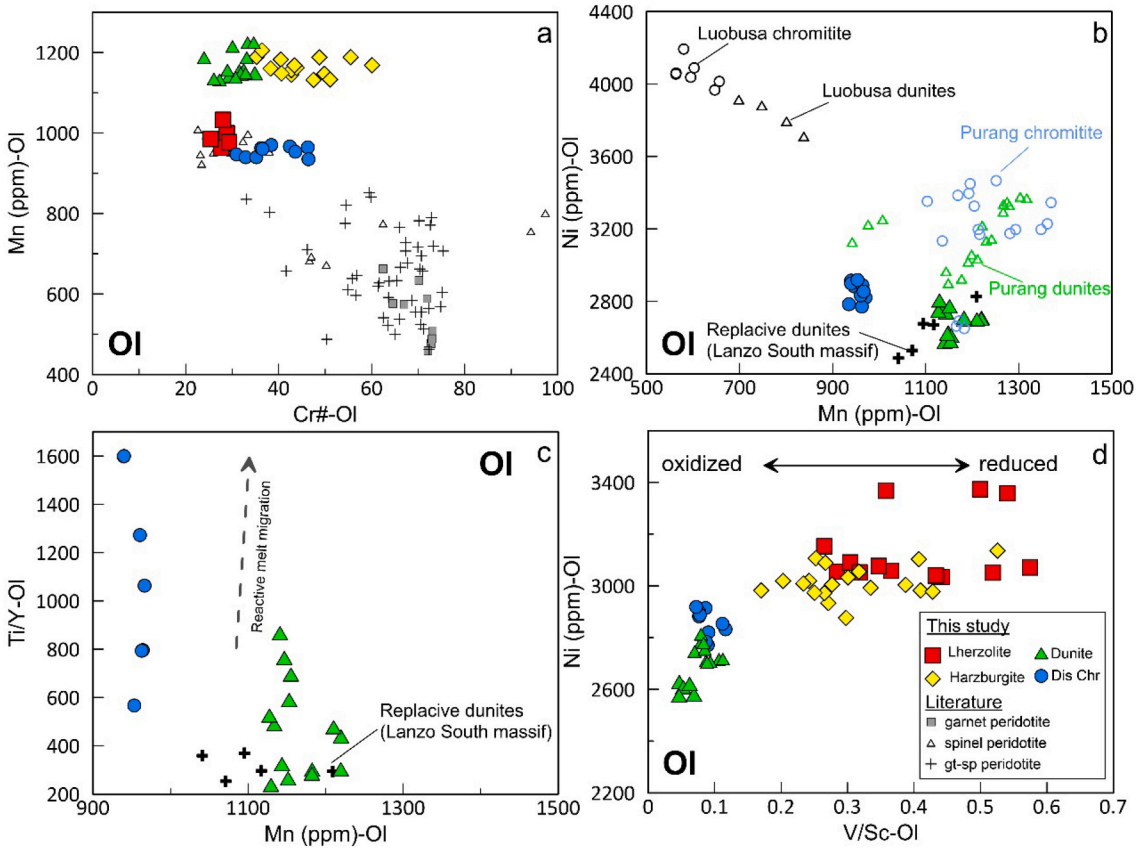

Fig. 7. Variations of Cr# (molar ratio 100*Cr/(Cr + Al)) vs. Mn (ppm) (a) of olivines from the Gomsiqe massif, Mirdita ophiolite. Mn (ppm) vs. Ni (ppm) (b), and Ti/Y ratios (c), in the olivines from Gomsiqe dunites and disseminated chromitites. The dashed gray arrow in Fig. 7c indicates variation in the Ti/Y ratios in samples resulted from interactions with melts. V/Sc ratios versus Ni (ppm) (d) of olivines from the Gomsiqe massif. V/Sc ratios are useful to infer oxidation state during partial melting. Metasomatized peridotites commonly exhibit lower V/Sc ratios of olivines (Foley et al., 2013). The data of olivines obtained from spinel-, garnet-, and garnet-spinel peridotite xenoliths (De Hoog et al., 2010; Witt-Eickschen and O'Neill, 2005), replacive dunites (Sanfilippo et al., 2014), dunites and chromitites from Purang and Luobusa ophiolites (Su et al., 2019) are also used for comparative purposes.

harzburgites, respectively, have variable and lower concentrations of the strongly incompatible lithophile elements than those of DMM (Workman and Hart, 2005), and negative anomalies in elements Sr, Zr, and Ti, whereas the Cpx in the dunites have variable positive anomalies in these elements, relative to neighboring elements (Fig. 8b).

4.2.3. Orthopyroxene (Opx)

REE abundances of the Gomsiqe lherzolitic and harzburgitic Opxs are depleted compared to those of Opxs from DMM (Fig. 8d; Table A9) (Workman and Hart, 2005). The Opxs chondrite-normalized REE patterns of the Gomsiqe lherzolites show similar features, but with higher total REE concentrations, in contrast to those in both Oman lherzolite types (Fig. 8d). Opxs in the Gomsiqe harzburgites are low in L-MREE concentrations (Fig. 8d), but show similar HREE concentrations to those in the Oman lherzolites. There is a clear difference between the REE patterns of Gomsiqe harzburgitic Opxs and those of Oman harzburgitic Opxs (Khedr et al., 2014).

4.2.4. Spinel (Spl)

Large variations are observed (Fig. A2) in the abundances of several trace elements between individual lithologies (Table S10). The distribution patterns of trace element contents of Spl grains from the dunites and disseminated chromitites are consistent with that of Spl in typical high-Al chromitites rather than typical high-Cr chromitites (Fig. A2a). Due to the similar properties of Ga and Al^{3+} (Page and Barnes, 2009), it is expected that the Ga content is negatively correlated with the Cr# values of Spl from individual lithologies (Fig. A2b).

4.3. Whole-rock major and trace-element compositions

4.3.1. Major and trace elements

The analyzed peridotite samples are Mg-rich (37.25–41.43 wt%), Al-poor (0.98–2.32 wt%), and Na-poor ($Na_2O < 0.08$ wt%) (Table A6). On the MgO/SiO_2 vs. Al_2O_3/SiO_2 plot (Fig. 9a), the Gomsiqe lherzolites and harzburgites are arranged along the terrestrial mantle array, whereas the dunites plot above the mantle array. In the Harker diagrams (Fig. 9b), the lherzolites and harzburgites show a relatively linear decrease in Al_2O_3 content with increasing MgO content, while the dunites do not follow this trend with elevated Al_2O_3 contents due to higher Al-rich spinel modal contents (Fig. 3). Additionally, lherzolites have lower abundances of Ni, compared to those of harzburgites and dunites (Fig. A3a). Y is negatively correlated with MgO among different Gomsiqe peridotitic lithologies (Fig. A3b). We have also included data on forearc, abyssal peridotites, and Oman ophiolitic peridotites in Fig. 9 for comparison. It is clear that the Gomsiqe lherzolite and harzburgite plot in the abyssal peridotite field (Fig. 9). Gomsiqe lherzolites are similar to Oman lherzolites (Khedr et al., 2014), but significantly differ from the Oman re-enriched harzburgites that have undergone melt metasomatic processes (Hanghøj et al., 2010).

4.3.2. Platinum group elements (PGE)

Whole-rock PGE concentrations are low in all samples (Table A6), and account for an average of 23.38 ppb in lherzolites, 20.17 ppb in harzburgites, and 10.63 ppb in dunites (except Du-prox. sample 16AS160). Lherzolite and harzburgite samples from the Gomsiqe massif

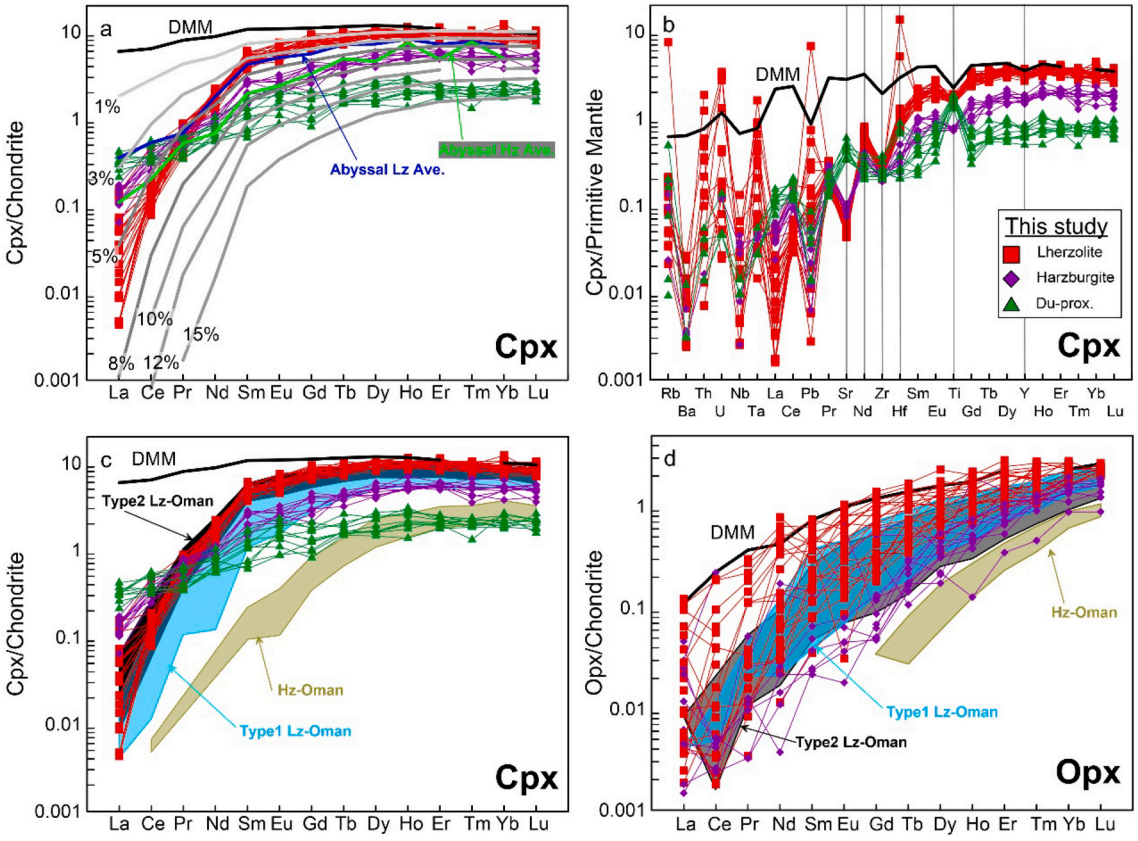

Fig. 8. (a) and (c) Chondrite-normalized (McDonough and Sun, 1995) REE patterns of Cpxs from the Gomsiqe massif, Mirdita ophiolite. Blue and green solid lines in Fig. 8a represent average composition of the abyssal lherzolitic and harzburgitic Cpxs, respectively, from Warren (2016); (b) Primitive mantle (PM)-normalized (McDonough and Sun, 1995) trace-elements spider diagrams of Opxs from the Gomsiqe massif, Mirdita ophiolite; (d) Chondrite-normalized REE patterns of Opxs from the Gomsiqe massif, Mirdita ophiolite. REE of Cpxs after 1, 3, 5, 8, 10, 12, and 15% fractional melting from DMM (Workman and Hart, 2005) are shown, following the theory proposed by Hellebrand et al. (2002). Data on Cpxs from Oman ophiolite were provided by Khedr et al. (2014). (For interpretation of the references to colour in this figure legend, the reader is referred to the web version of this article.)

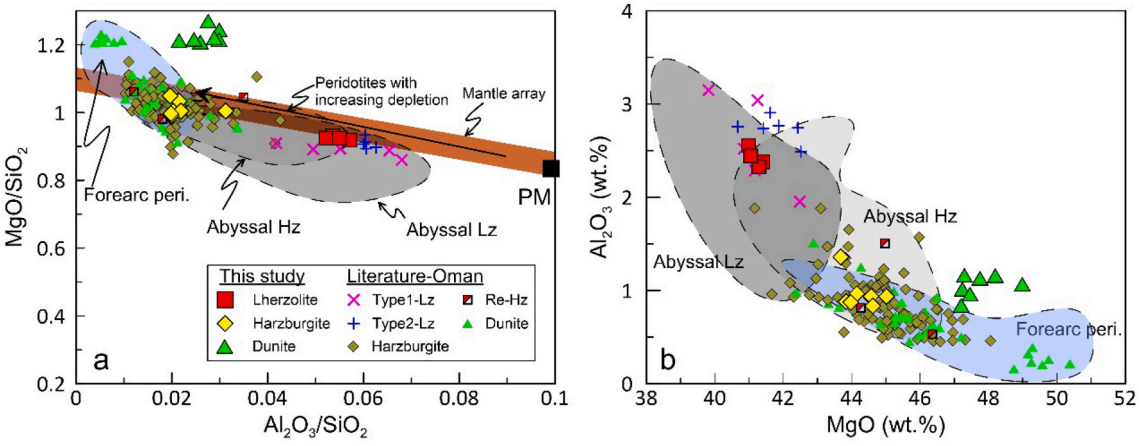

Fig. 9. (a) Whole-rock (WR) MgO/SiO_2 vs. Al_2O_3/SiO_2 of the Gomsiqe peridotites, Mirdita ophiolite. Peridotite depletion trends and primitive mantle (PM) are proposed by Snow and Dick (1995) and McDonough and Sun (1995), respectively; Variation diagrams of MgO (wt%) vs. Al_2O_3 (wt%) (b) in Gomsiqe peridotites, Mirdita ophiolite. Regions of abyssal peridotites (Abyssal Lz and Hz) (Warren, 2016) and forearc peridotites (Forearc peri.) (Ishii et al., 1992; Parkinson and Pearce, 1998) are exhibited for comparative purpose. Data for Oman ophiolite are from the same references used in Fig. 5.

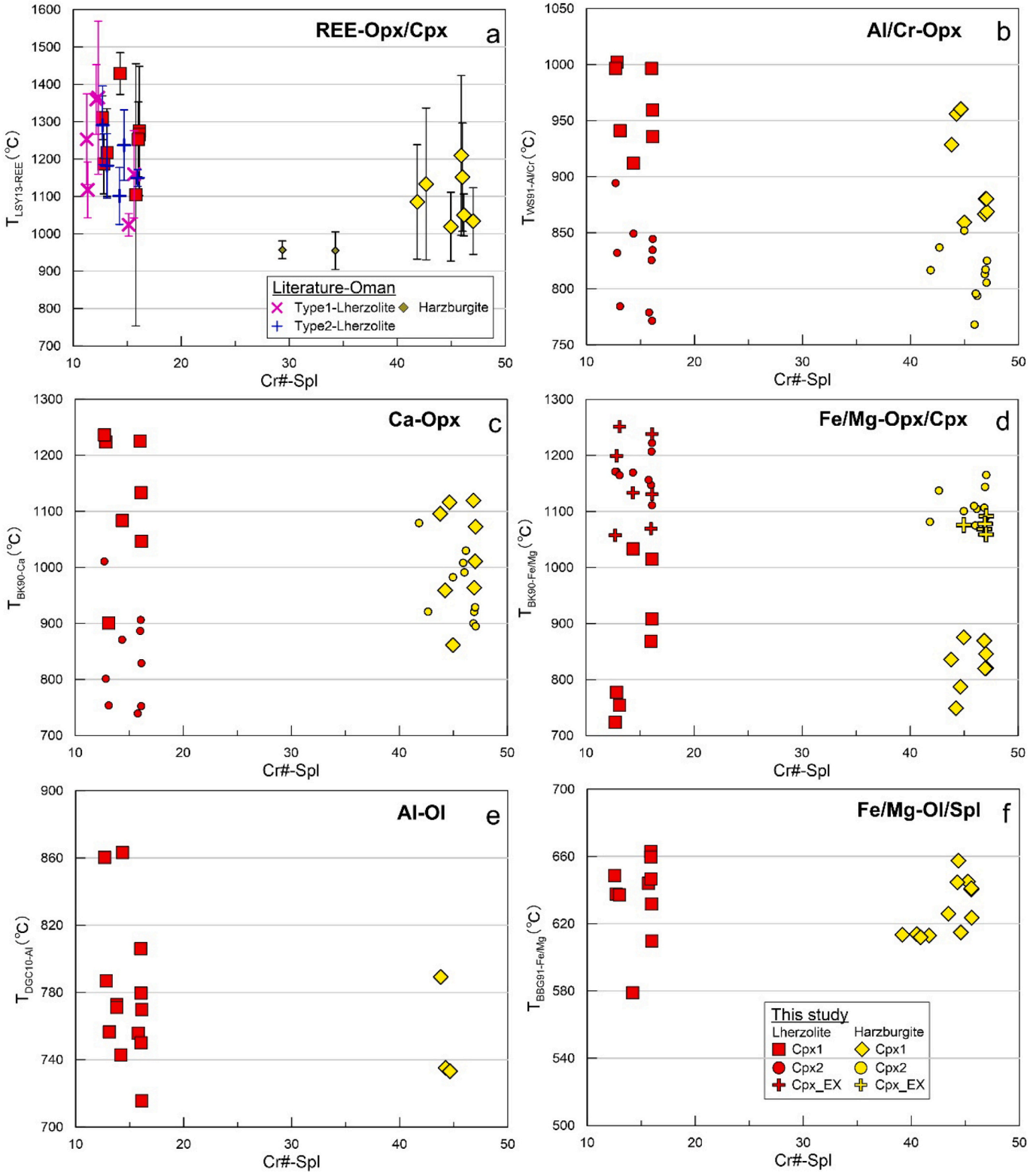

Fig. 10. Variations of spinel Cr# vs. estimated temperatures derived from different thermometers (a, $T_{LSY13-REE}$; b, $T_{WS91-Al/Cr}$; c, $T_{BK90-Ca}$; d, $T_{BK90-Fe/Mg}$; e, $T_{DGC10-Al}$; f, $T_{BBG91-Fe/Mg}$) for mineral pairs in the Gomsiqe massif, Mirdita ophiolite. The error bars in Fig. 10a are ±1σ. Data of Oman ophiolite are from Khedr et al. (2014).

show consistent primitive mantle (PM)-normalized PGE patterns (Fig. A4; McDonough and Sun, 1995), whereas the PGE concentration in dunites is much lower than that of PM (Fig. A4; McDonough and Sun, 1995). In detail, Du-prox. are significantly enriched in PGE abundances compared with the Du-distal., and show enrichment in the palladium subgroup PGE (PPGE, including Rh, Pt, and Pd) relative to the iridium subgroup PGE (IPGE, including Os, Ir, Ru). Disseminated chromitites (Dis Chr) have higher PGE contents (176.61 ppb) than other Gomsiqe lithologies.

4.4. Temperature estimates

We calculated equilibrium temperatures of Gomsiqe lherzolites and harzburgites at 1.5 GPa (spinel-facies peridotites) (Fig. 4; Table A12). We chose thermometers applied in different major forming-rock minerals for mantle rocks: (1) $T_{LSY13\text{-}REE}$ (REE-in-two-pyroxene; Liang et al., 2013); (2) $T_{WS91\text{-}Al/Cr}$ (Al—Cr exchange-in-Opx; Witt-Eickschen and Seck, 1991); (3) $T_{BK90\text{-}Ca}$ (Ca-in-Opx; Brey and Kohler, 1990); (4) $T_{BK90\text{-}Fe/Mg}$ (Fe—Mg exchange between Opx and Cpx; Brey and Kohler, 1990); (5) $T_{DGC10\text{-}Al}$ (Al-in Ol, De Hoog et al., 2010), and (6) $T_{BBG91\text{-}Fe/Mg}$ (Fe—Mg exchange between Ol and Spl, Ballhaus et al., 1991).

The $T_{LSY13\text{-}REE}$ thermometer, based on REE exchange between coexistent Opx and Cpx, usually exhibits the highest equilibrium temperatures (Fig. 10a), whereas thermometers ($T_{WS91\text{-}Al/Cr}$, $T_{BK90\text{-}Ca}$, $T_{BK90\text{-}Fe/Mg}$) based on major-element exchanges in pyroxenes exhibit lower temperatures (Fig. 10b–d). Thermometers on the basis of Al in olivine ($T_{DGC10\text{-}Al}$) and Fe—Mg exchanges between coexistent Ol and Spl ($T_{BBG91\text{-}Fe/Mg}$) exhibit the lowest temperatures (Fig. 10e–f). Pyroxene thermometers indicate that the Gomsiqe lherzolites generally have higher equilibrium temperatures than the harzburgites (Fig. 10a–d), whereas thermometers based on Ol and Spl commonly exhibit comparable temperatures in both peridotite types (Fig. 10e–f). The $T_{LSY13\text{-}REE}$ thermometers on the basis of the porphyroclastic Opx-Cpx pairs in the lherzolites have the highest temperature estimates (1104–1429 °C; Fig. 10a), similar to that in the Oman basal lherzolites (1024–1364 °C; Fig. 10a; Khedr et al., 2014). The Gomsiqe harzburgites exhibit higher temperatures using the $T_{LSY13\text{-}REE}$ thermometer, compared with the Oman harzburgites (Fig. 10a; Khedr et al., 2014). As for the Gomsiqe lherzolites, Cpx exsolution (Cpx_EX) within Opx porphyroclasts (Opx1) usually exhibit the highest temperatures (up to 1236 °C; Fig. 10d), followed by those of porphyroclastic Opx1-Cpx1 pairs, and the lowest temperatures are recorded by the Opx2-Cpx2 mineral pairs (Fig. 10b–c). Abnormally, the thermometer ($T_{BK90\text{-}Fe/Mg}$) based on mineral pairs of Opx2 and Cpx2 exhibit higher temperature estimates than those based on porphyroclastic Opx1-Cpx1 pairs (Fig. 10d).

5. Discussion

5.1. Gomsiqe basal lherzolites in the lower part of the mantle section: A less refractory lithospheric mantle after low degrees of melting of the asthenosphere rather than refertilization origin

Basal lherzolites were reported in the Oman ophiolite in different massifs (i.e., Fizh block in the northern and Wadi Sarami in the central), and had experienced strong deformation (Khedr et al., 2014; Takazawa et al., 2003), which is similar to the petrographic features of the basal lherzolites found in the Gomsiqe massif, as previously mentioned (Figs. 2, 3). However, some researchers have proposed that the Fizh basal lherzolites formed via refertilization of refractory peridotite by freezing of trapped melts, i.e., spoon-shaped REE pattern of Cpx and Ti enrichment in Spl (Takazawa et al., 2003), while the Wadi Sarami basal lherzolites were free of evidence of melt refertilization in chemistry, e.g., as those shown in the Fizh basal lherzolites aforementioned, and in texture, e.g., veins of interstitial Cpx around porphyroclast grains, and indicated intrinsic mantle heterogeneity (Khedr et al., 2014).

In present study, Cpx grains in Gomsiqe basal lherzolites do not show evidence of melt refertilization in mineral geochemistry, for example, relative enrichment of L-MREE in Cpx with spoon-shaped REE patterns (Seyler et al., 2007), and relative enrichment of HFSE compared to neighboring elements. In contrast, in Fig. 8, Gomsiqe lherzolitic Cpx grains are severely depleted in LREE, which is typically consistent with those in abyssal lherzolites (Warren, 2016), and Wadi Sarami type 2 lherzolites, Oman ophiolite (Khedr et al., 2014), and show depleted HFSE characteristics, such as Zr, Ti, and Y, relative to neighboring elements. The porphyroclastic Cpx1 in basal lherzolites exhibit negative correlations between Al and Cr (Fig. 5e), which are assumed to be formed during partial melting (Pan et al., 2022). Moreover, there are evident differences between the Gomsiqe basal lherzolites and the Oman re-enriched harzburgites based on whole-rock geochemistry (Fig. 9; Hanghøj et al., 2010). In addition, Cpxs in Gomsiqe basal lherzolites are free of evidence of melt refertilization in petrographic features, e.g., wormy or thin veins of interstitial Cpx grains around porphyroclast minerals. Hence, the refertilization origin of Gomsiqe lherzolites can be excluded. In fact, ridge axes were inferred near the Gomsiqe massif (Fig. 1; Nicolas et al., 1999), a tectonic setting that should preserve primitive fertile asthenospheric entities at the base of the oceanic lithosphere.

5.2. Mantle heterogeneity resulting from variation of partial melting

The petrographic investigations on the Gomsiqe peridotites show that the basal lherzolites exhibit obvious plastic deformation at high temperatures (Fig. 4a-b), orthopyroxene porphyroclasts with clinopyroxene + Al-spinels exsolution (Fig. 4e-g) and sulfides inclusions (i.e., pentlandite; Fig. 4e–f). In contrast, the harzburgites exhibit low modal contents of Cpx (Figs. 3 and 4), less high-temperature deformation (Fig. 4) and much less occurrence of sulfide inclusions within Opx porphyroclasts. These petrographic features are consistent with the differences in chemical compositions and equilibration temperatures between the two types of peridotites.

Although re-equilibration during the sub-solidus cooling process (Xiong et al., 2017b) may alter the composition of Cpx2 grains with lower Al_2O_3, Na_2O, and Cr_2O_3, but slightly higher Mg#, than those of Cpx1 in both Gomsiqe lherzolites and harzburgites (Fig. 5). Owing to their fusible chemical properties, the Al_2O_3 and Na_2O contents of porphyroclastic Cpx1 within the Gomsiqe peridotites (basal lherzolites and harzburgites, respectively) decrease with increasing Mg# values, which can be regarded as a proxy for the extent of partial melting of mantle rocks (Fig. 5c–d; Warren, 2016). Additionally, the relative depleted characteristics of M-HREE (Fig. 8a) and HFSE (that is, Hf, Ti; Fig. A5) in the porphyroclast Cpx indicates a more refractory nature of the Gomsiqe harzburgites relative to the lherzolites (Hellebrand et al., 2002; Pearce et al., 2000; Warren, 2016). These elements in residual clinopyroxenes can impose constraints on the melting history of mantle peridotites by partial melting model calculations (Johnson et al.,1990). In general, it can be observed in Fig. 8 that the Gomsiqe basal lherzolites and harzburgites have relatively flat M-HREE patterns, corresponding to ~3–5% and ~ 8–10%, respectively, i.e., pure fractional melting of DMM (Workman and Hart, 2005) within the spinel stability field. By using Dy vs. Ti covariation of Cpx for modeling proposed by Bizimis et al. (2000), most of the Cpxs from the basal lherzolites plot in the region of abyssal lherzolites (Fig. 12a). This finding can be taken to represent residues after ~3% anhydrous melting of a DMM source, comparable to the Wadi Sarami lherzolites, especially the Type 2 lherzolites (Khedr et al., 2014). In contrast, Gomsiqe harzburgites show a higher extent (~8–10%) of anhydrous partial melting, consistent with abyssal harzburgites (Fig. 12a).

With a higher extent of partial melting, the Cr# of Spl within host rocks is expected to be higher, as well as the Mg# of Spl (Arai, 1994; Fig. 6a–b). Thus, the higher Cr# of the Gomsiqe harzburgitic Spl than those of lherzolitic Spl indicates a more refractory nature, which is consistent with inferences from Cpx geochemistry. Quantitatively

speaking, the Gomsiqe lherzolites and harzburgites have undergone ~3–5% and ~ 14–16% degree of melting (F_{min}), respectively (Hellebrand et al., 2002). Coexistent spinel-olivine compositional relationships (Cr# in Spl vs. Fo in Ol) further confirms that the Gomsiqe harzburgites represent relics of higher degrees of melt extraction than those of lherzolites (Fig. 13a).

Olivine is the major host mineral of some trace elements, such as Ni (ca. 90% hosted in Ol) and Mn (ca. 50%) (De Hoog et al., 2010; Sanfilippo et al., 2014). Here, we chose the compatible elements Ni and Mn in olivine as the parameters of peridotite fertility (De Hoog et al., 2010). The Cr# of olivine is strongly positively correlated with that of coexistent Spl in all peridotite types (Fig. A1a; De Hoog et al., 2010), so a negative correlation between Ni, Mn, and Cr# in olivine is expected. Ni concentrations decrease with increasing Cr# values of olivine, indicating a higher degree of depletion (Fig. A1b), which is consistent with the previous inference. However, the correlation between Mn concentrations and Cr# values in Gomsiqe lherzolitic and harzburgitic olivines does not follow the trend shown by Ni (Fig. 7a). Higher degree of partial melting cannot produce such chemical variations of Mn in olivines from Gomsiqe harzburgites.

These above findings imply that Gomsiqe harzburgites sustained a higher extent of melt extraction than that of the basal lherzolites. Other evidence in support of this inference includes: (1) the relatively lower Al_2O_3 abundance in harzburgitic Opx1 (Fig. 5b); (2) the relatively lower HREE concentration in harzburgitic Opx (Fig. 8); (3) the progressive depletion of harzburgites illustrated by whole-rock major oxides (e.g., Al_2O_3; Fig. 9b) and HFSE (e.g., Y; Fig. A3b); and (4) the elevated whole-rock compatible trace element (e.g., Ni; Fig. A3a) in Gomsiqe harzburgites.

All the above estimates based on the assumption that melting occurs in the Spl stability field. However, in Fig. 12, the majority of the Gomsiqe lherzolites and harzburgites are situated below the modeling trajectory of fractional melting alone in the spinel facies. Thus, it is inferred that the Gomsiqe lherzolites sustained 1–7% garnet (grt) facies melting prior to 1–5% spinel (spl)-facies melting, while the harzburgites underwent 2–4% grt-facies melting before 7–10% spl-facies melting. Similar characteristics have been reported for abyssal peridotites from the MAR (Seyler et al., 2007), ophiolitic peridotites from Tibet, China (e.g., Xigaze and Purang; Liu et al., 2019) and Oman (Khedr et al., 2014), and have been explained to be the result of initial grt-facies melting preceding subsequent spl-facies melting (Hellebrand et al., 2002; Johnson et al., 1990).

Warren (2016) argued that the low $(Sm/Yb)_N$ values of Cpx from abyssal peridotites result from the redistribution of trace elements between Cpx and other silicate minerals during sub-solidus re-equilibration(i.e., exsolution of Opx from Cpx and vice versa) and uncertainties in model parameters, rather than initial garnet-facies melting. Indeed, REE in lherzolitic clinopyroxene is immune to sub-solidus re-equilibration compared to Cpx within highly depleted harzburgite (Liang et al., 2021). And Gomsiqe harzburgites experienced a small to moderate extent of melting. Additionally, given the high similarity between the Gomsiqe basal lherzolites and the Wadi Sarami type 2 basal lherzolites (Khedr et al., 2014), we prefer the two-stage melting explanation (i.e., initial grt-facies melting prior to subsequent spl-facies melting).

5.3. Melt-rock interaction

Melt-rock interaction is an important process recorded by the abyssal peridotites, and is one of the main causes of mantle heterogeneity (Warren, 2016). As for the Gomsiqe samples, melt-rock interaction was originally demonstrated by the occurrence of reactive petrographic microtextures within the harzburgites and dunites, whereas basal lherzolites are almost completely unaffected by such melt metasomatism. In particular, fine olivine+clinopyroxene neoblasts embayed at the margin of the harzburgite porphyroclastic orthopyroxenes imply the consumption of Opx and the subsequent formation of Ol and Cpx during melt-rock interaction (Fig. 4j–k). This petrographic feature results from the interplay between mantle peridotites and silica-undersaturated melts (Pearce et al., 2000; Seyler et al., 2007).

Because LREEs are more fusible than HREEs during the partial melting process, it is expected that the more depleted harzburgitic Cpx should have lower LREE concentrations compared to those in the basal lherzolites. The observed chondrite-normalized REE patterns, however, exhibit elevated LREE (Fig. 8a), indicating that the Gomsiqe harzburgites are melting residues, but also have sustained late-stage melt metasomatism. In Fig. 11a, the hypothetical equilibrated melts calculated from harzburgitic Cpxs have REE patterns and abundances similar to the Izu-Bonin-Mariana forearc basalts. The porphyroclastic Cpx1 minerals in harzburgites exhibit positive correlations between Al and Cr (Fig. 5e), which indicates a robust chemical proxy for the metasomatism

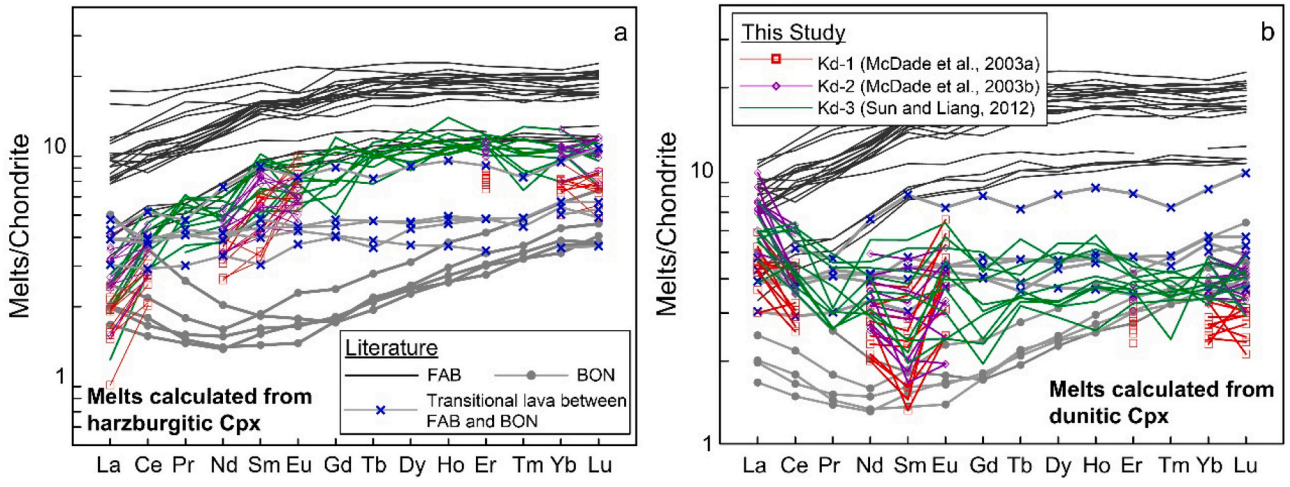

Fig. 11. Chondrite-normalized REE patterns of hypothetical melts equilibrated with Cpxs in Gomsiqe harzburgites (a), and dunites (b). Partition coefficients of REE between Cpxs and basaltic melts are acquired by different experiments under different conditions. Kd-1 is proposed by McDade et al. (2003a) (1315 °C, 1.5 GPa, equilibrated with an anhydrous high-MgO basaltic melt); Kd-2 is proposed by McDade et al. (2003b) (1245 °C, 1.3 GPa, equilibrated with a hydrous (1.5 wt% H_2O) high-MgO basaltic melt); and Kd-3 is determined by Sun and Liang (2012) (1300 °C, spinel stability field, equilibrated with an anhydrous basaltic melt). These experimental conditions can cover a wide range of temperatures (1245 to 1315 °C) and estimate the water effect (hydrous vs. anhydrous) on REE distribution between Cpxs and basaltic melt. These experiments are conducted at typical pressure conditions (1.3–1.5 GPa) assumed for spinel-facies peridotites. Cpx REE patterns of forearc basalts (FAB), transitional lava between FAB and BON, and boninites (BON) of the IBM arc (Reagan et al., 2010) are also plotted for comparative purposes.

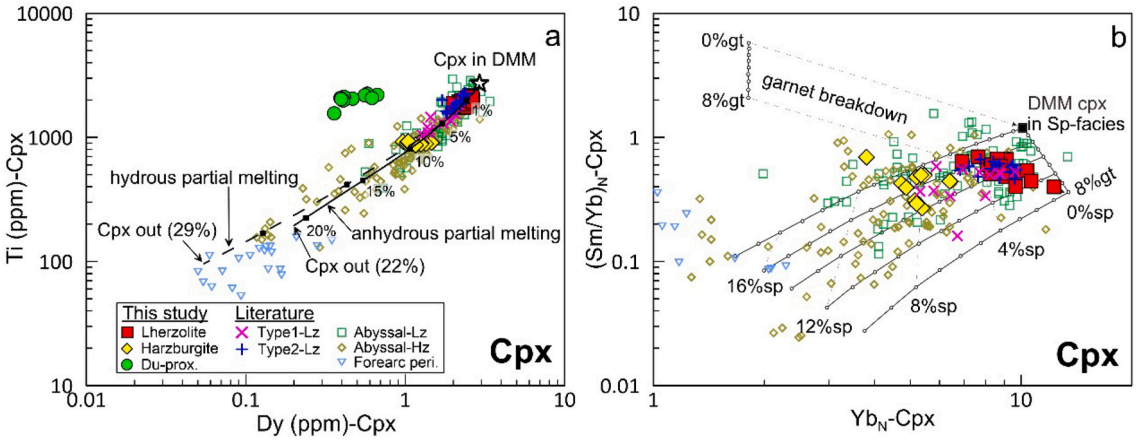

Fig. 12. (a) Variations of Dy (ppm) vs. Ti (ppm) for Cpxs in the Gomsiqe peridotites, Mirdita ophiolite. Modeling theory are proposed by Bizimis et al. (2000). (b) Chondrite-normalized $(Sm/Yb)_N$ vs. $(Yb)_N$ for Cpxs in the Gomsiqe peridotites, Mirdita ophiolite. The modeled melting curves are proposed by Hellebrand et al. (2002). Data source for abyssal peridotites (abyssal lz and hz), forearc peridotites (forearc peri.), and Oman lherzolites (type1 and type2 lz) are same as in Fig. 5.

(Pan et al., 2022). Additionally, spinels in harzburgites are similar in composition to spinels in MORB (Fig. 6b and d), and have higher TiO_2 contents than Spl in Oman harzburgites and the majority of abyssal peridotites (Fig. A6); these spinels deviate from the partial melting trend (Fig. 6c). The Gomsiqe harzburgitic olivines show higher Mn concentrations associated with higher Cr# values compared to the lherzolitic olivines (Fig. 7a). We suggest that elevated Mn concentration in harzburgitic olivines may result from melt-rock interaction as the MORB-like melts contain Mn (Sanfilippo et al., 2014). This can be inferred because that MORB genesis involves the consumption of garnet-bearing material in their mantle source under low pressure condition (Sobolev et al., 2007). Thus, both Cpx, Spl and Ol compositions suggest that Gomsiqe harzburgites equilibrated with liquids similar to forearc basalts (MORB-like), consistent with the inference of Liang et al. (2010), that is, the lower part of a high-porosity channel in the mantle is harzburgite.

Dunite lenses within upper mantle rocks of ophiolites are commonly interpreted as melt channels resulting from interactions between mantle peridotites and Si-unsaturated melts (Kelemen et al., 1995; Xiong et al., 2017b). However, the dunites contain higher MgO (Fig. 9), and lower CaO, a more depleted HREE content of Cpx (Fig. 8a), and a much lower proportion of pyroxenes relative to hosting harzburgites. These chemical and petrographic characteristics suggest that the low-Cr# Gomsiqe dunites and some clinopyroxenes within them have preserved or inherited the chemical signatures of the depleted harzburgites, which were the reactant protoliths for the low-Cr# dunites and chromitites (e.g., González-Jiménez et al., 2014; Kelemen et al., 1995).

In terms of the spinel compositions in the dunites, however, they exhibit slight lower Cr# values (34.0–40.9 vs. 40.6–47.1, respectively) and higher TiO_2 contents (0.15–0.30 wt% vs. 0.08–0.21 wt%, respectively) than those of the spinel in hosting harzburgites (Fig. 6c). Moreover, the veinlet texture of Cpx grains (Fig. 4l) and the flat REE pattern with a gentle slope of LREE of clinopyroxenes in Gomsiqe dunites (Fig. 8) are consistent with that of magmatic clinopyroxene crystallized from MORB-like melt (Akizawa et al., 2012; Seyler et al., 2001, 2007). The observed relative enrichment of LREE (Fig. 8) and incompatible elements (i.e., Sr, Zr, and Ti) in dunitic Cpxs with respect to neighboring elements (Fig. 8), and the obvious deviation from the melting curve (Fig. 12a) can result from melt metasomatism with mantle rocks (Kelemen et al., 1995; Pearce et al., 2000). Despite this, the melt metasomatism mechanism can account for the enrichment of Zr, Ti (high field strength elements (HFSE), fluid immobile) enrichment (Fig. 12), but fails to explain the Sr (fluid mobile element) enrichment (Fig. 8b), as large ion lithophile elements (LILE) are more mobile in hydrous fluids (Bizimis et al., 2000; Kelemen et al., 1995; Pearce et al., 2000).

The Sr (hydrophile element) enrichment of clinopyroxenes in dunites implies refertilization by hydrous fluid influx (Fig. 8) (Bizimis et al., 2000). Supporting this inference is the occurrence of hydrous mineral inclusions (pargasite and phlogopite) in the spinels of the dunites (Fig. 4). The incongruent melting of orthopyroxene (e.g., Pearce et al., 2000; his reaction 5: orthopyroxene+melt1 = olivine+clinopyroxene+melt2) increases under hydrous conditions, which also results in the crystallization of clinopyroxene. On the other hand, the theoretical melts equilibrated with these Cpxs in Gomsiqe dunites have patterns and abundances similar to IBM lavas transitional between forearc basalts (FAB) and boninites (BON) (Fig. 11b), which contain more fluid-soluble elements due to fluid fluxing from the subducting slab, than spreading center lavas (Reagan et al., 2010). Here, we infer that the metasomatic agent that modifies the harzburgite differs from that interacting with the dunites. The latter is also a MORB-like melt, but with more hydrous (still rare) fluid involved.

5.4. *Thermal-state variation during subduction initiation recorded by the Gomsiqe mantle peridotites*

Some Opx porphyroclasts in the basal lherzolites contain exsolved lamellae of clinopyroxenes and Al-spinels (Fig. 4f–g), which are also found in Oman basal lherzolites (Khedr et al., 2014). Such feathers, which are commonly absent in the Gomsiqe harzburgites, generally indicate higher temperatures and pressure conditions recorded by the basal lherzolites compared to the harzburgite.

Because of the much slower diffusion rates of trivalent cations (e.g., REE^{3+} and Cr^{3+}-Al^{3+}) than divalent cations (e.g., Ca^{2+} and Mg^{2+}-Fe^{2+}) during sub-solidus cooling (Liang et al., 2013), the thermometers based on trivalent cations are more reliable in estimating the primitive thermal conditions of the mantle. In terms of the porphyroclast Cpx-Opx mineral pairs, different thermometers all give higher (~100–200 °C) estimated temperatures of lherzolites than those of harzburgites (Fig. 10). The closure temperatures given by the REE thermometer (average of 1255 °C) of Gomsiqe basal lherzolites are comparable with that of the Oman Type 2 basal lherzolites (1101–1291 °C; Fig. 10a), which likely represent a less refractory lithospheric mantle after low degrees of melting of the asthenosphere (Khedr et al., 2014). In view of fact that the potential temperature of Phanerozoic mantle is ~1350 ± 50 °C (Herzberg et al., 2010), we suggest that the Gomsiqe lherzolites may preserve the primitive thermal state just after upwelling and adiabatic decompression melting. The variations in closure temperatures estimated by

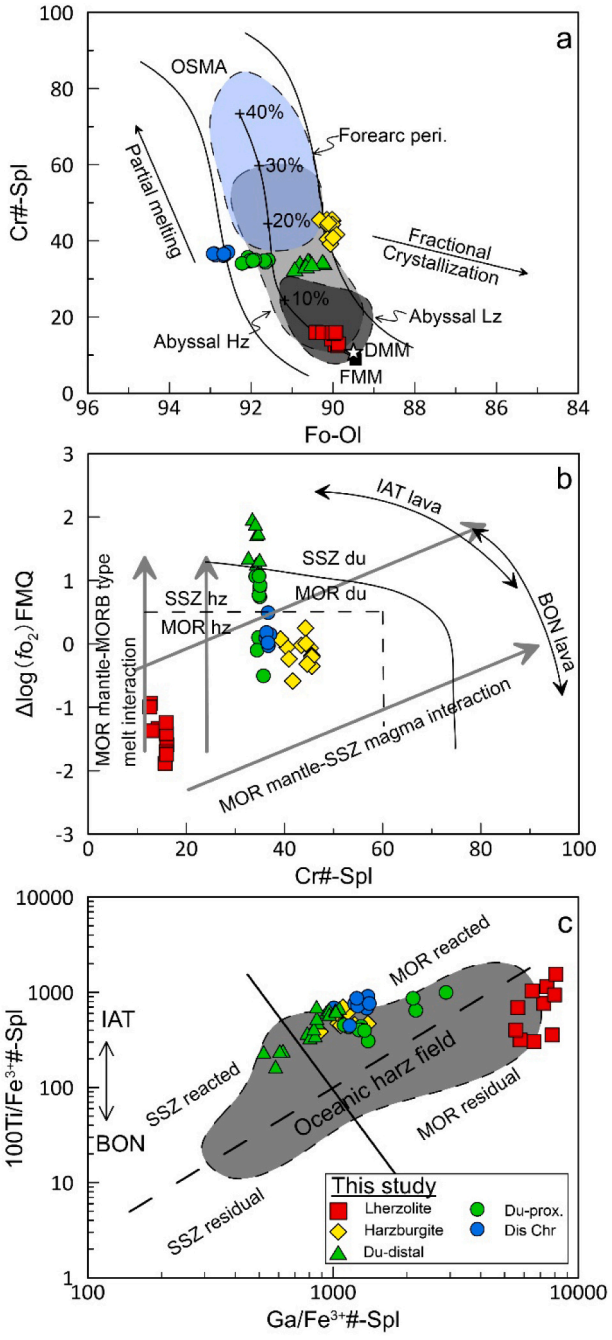

Fig. 13. Variations of Fo in Ol vs. Cr# in coexistent Spl (a), Cr# in Spl vs. $\Delta\log fo_2$ (b), and Ga/Fe^{3+}# vs. Ti/Fe^{3+}# in Spl (c) from the Gomsiqe massif, Mirdita ophiolite. The modeled melting curves in (a) are from Wu et al. (2018). The olivine-spinel mantle array (OSMA) is proposed by Arai (1994). The discrimination boundaries in (b) and (c) are obtained from Dare et al. (2009). Data sources of abyssal lherzolites (abyssal lz) and harzburgites (abyssal hz), forearc peridotites (forearc peri.) are same as those in Fig. 5. Abbreviations: BON-boninite; FMM-fertile mid-ocean ridge mantle; IAT-island arc tholeiite.

the REE thermometer (Fig. 10a) may be caused by the incomplete diffusive re-equilibration of REE between coexistent pyroxene mineral pairs due to rapid cooling (Liang et al., 2021). The generally higher closure temperatures in basal lherzolites are due to their lower stratigraphic level.

Cpx exsolution (Cpx_EX) lamellae within Opx porphyroclasts (Opx1) usually preserve the original thermal state of the Gomsiqe peridotites and provide relatively high temperatures, followed by those of Cpx1 and Opx1 porphyroclast mineral pairs, then by the mineral pairs in the matrix (Opx2 and Cpx2), as also demonstrated by the Zedang ophiolites (Xiong et al., 2017b). However, the Gomsiqe sample thermometer based on Fe—Mg exchange in mineral pairs of Opx2 and Cpx2 clearly gives higher temperature estimates than those in the porphyroclastic pairs of Opx1 and Cpx1 (Fig. 10d), consistent with the temperatures estimated based on Ca in Opx (Fig. 10c). This abnormal observation can be readily explained by the faster (one to two orders of magnitude larger) diffusivities of Ca, Mg, and Fe than the diffusivities of trivalent cations (e.g., REE^{3+} and Cr^{3+}-Al^{3+}) in pyroxene (Liang et al., 2013, 2021). If the juxtaposition Gomsiqe lherzolites and harzburgites experienced subsequent heating to ~1150 °C at the base of the oceanic lithosphere after their formation, to the first order, we would expect a quick re-equilibration for the 2^+ cations (such as Ca, Fe, and Mg) between Opx and Cpx, while the 3^+ cations remain the same. The relatively smaller grain size of the mineral pairs Opx2 and Cpx2 than the porphyroclastic mineral pairs of Opx1 and Cpx1 (Fig. 4) would be conducive for attaining equilibrium. Additionally, positive correlations of Al_2O_3 content and Mg# values in coexisting orthopyroxenes and clinopyroxenes (Fig. A7) indicate chemical equilibrium between these phases (Beard et al., 2007).

5.5. Mantle process inferred from oxygen fugacity and PGE behavior

5.5.1. Oxygen fugacity

The mantle oxygen fugacity (fo_2) of the Gomsiqe ultramafic body was estimated based on coexisting olivine and spinel (Table A11; Ballhaus et al., 1991):

$6Fe_2SiO_4$ (olivine) + O_2 (fluid) = $3Fe_2Si_2O_6$ (orthopyroxene) + $2Fe_3O_4$ (spinel).

The oxidation states of the investigated basal lherzolites (−1.88 < FMQ < -0.93) and harzburgites (−0.58 < FMQ < +0.25) are comparable with those of modern reduced oceanic mantle (Fig. 13b) (Dare et al., 2009; Parkinson and Arculus, 1999). The dunites (including disseminated chromitites), on the other hand, are obviously more oxidized (−0.50 < FMQ < +1.93) (Fig. 13b), straddling the MOR and SSZ dunite border. In detail, the Du-distal (i.e., sample 16AS158; Fig. 3) is apparently more oxidized (+1.09 < FMQ < +1.93) compared to Du-prox. (i.e., sample 16AS162, −0.50 < FMQ < +1.59) and disseminated chromitites (−0.03 < FMQ < +0.49). Such decrease in fo_2 from the Du-distal to the Du.prox. and chromitites is probably related to the chromitite-forming processes and preferably construed as the result of the exsolution of oxidized fluids from more oxidized magmas during subduction initiation (He et al., 2021; Su et al., 2020).

To further evaluate the effect of the extent of melt-rock interaction and the composition of the reacting melts on oxygen fugacity, the Ti/Fe^{3+}# vs. Ga/Fe^{3+}# [Fe^{3+}/(Fe^{3+} + Cr + Al)] diagram can to provide us with more information in conjunction with the fo_2–Cr# discrimination plot (Dare et al., 2009). Following the guidelines proposed by Dare et al. (2009), in Fig. 13c, we clearly see that the basal lherzolites represent the MOR residual mantle without reaction with melts, whereas the harzburgites represent the MOR-reacted mantle, as inferred in the previous section. Gomsiqe Du-distal straddles the region of SSZ-reacted and MOR-reacted oceanic peridotites, indicating the involvement of hydrous fluids during their formation (Fig. 4m) (Su et al., 2020), and equilibration with IBM lavas transitional between forearc basalts (FAB) and boninites (BON) (Fig. 11b). Gomsiqe Du-prox. and the disseminated chromitites all plot in the field of MOR-reacted oceanic peridotites (Fig. 13c), which is consistent with the decrease in fo_2 from the Du-distal to the Du.prox. and chromitites as shown in Fig. 13b.

5.5.2. Platinum group elements behavior

Gomsiqe basal lherzolites and harzburgites have relatively flat chondrite-normalized PGE patterns, consistent with those of PM (Fig. A4), indicating limited extent of partial melting and melt addition, as discussed in previous sections. The Du-distal samples have lower PGE

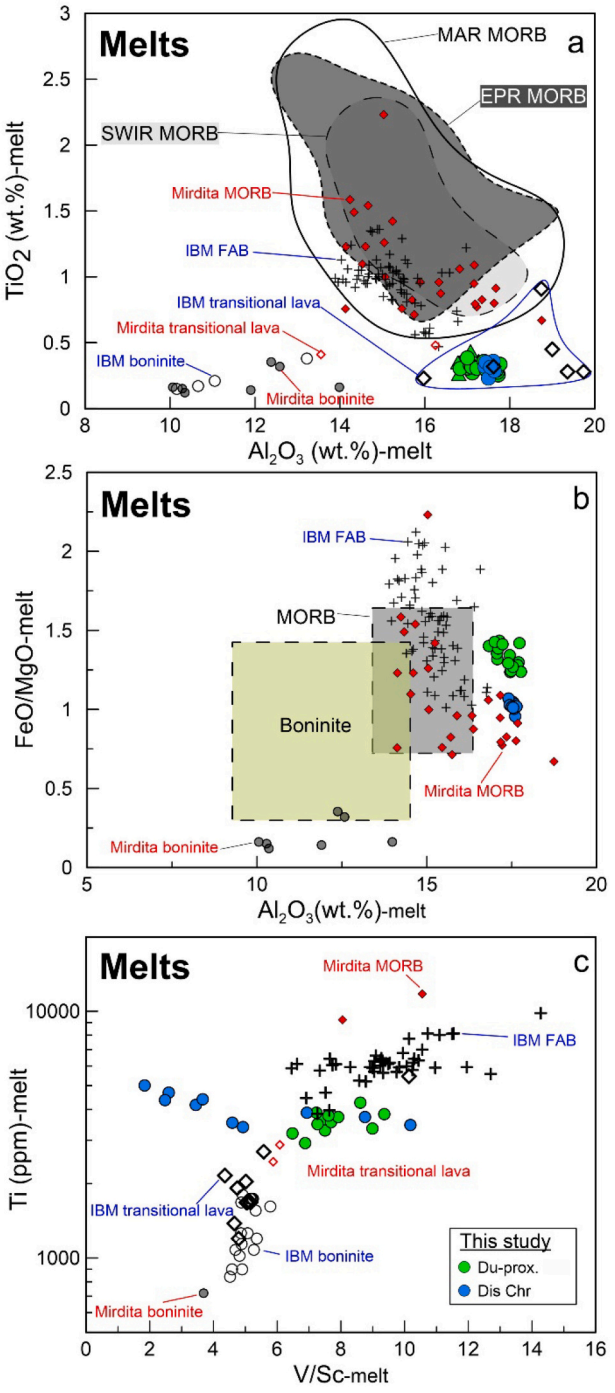

Fig. 14. Variations of Al_2O_3 (wt%) vs. TiO_2 (wt%) (a), $(FeO/MgO)_{melt}$ (b), and $(V/Sc)_{melt}$ vs. Ti (ppm) (c) of the calculated parental melts of dunites and disseminated chromitites in the Gomsiqe massif, Mirdita ophiolite. Data of SWIR, MAR, and EPR MORB in (a) are from Gale et al. (2013). Data of Mirdita MORB, transitional lava, and boninites are from Dilek et al. (2008) and Saccani et al. (2018). Data of IBM forearc basalts (FAB), transitional lava between FAB and boninites (BON), and BON are from Reagan et al. (2010); Discrimination areas of MORB and boninite in (b) are obtained from Barnes and Roeder (2001).

contents relative to PM (Fig. A4). This phenomenon is consistent with the more depleted nature of the dunites as evidenced by the more depleted feature of HREE of dunitic Cpxs, compared to those of the harzburgitic Cpxs (Fig. 8). In contrast, Du-prox. Samples and disseminated chromitites have higher PGE compositions due to the presence of more spinel (Fig. 3), and display PPGE-rich patterns similar to those of interstitial sulfides (Fig. A4), supporting a replacive origin (Alard et al., 2000; Woodland et al., 2002). S-undersaturated melts (e.g., boninitic magmas) interact with the reacting peridotites to dissolve interstitial sulfides and generate depletion of PPGEs in them (Liu et al., 2019; Xiong et al., 2017b; Zhou et al., 2014). The chondrite-normalized PPGE-rich patterns of Gomsiqe Du-prox. and chromitites (Fig. A4) indicate that melts that interacted with the peridotites were sulfur-saturated. This type of S-saturated melt (i.e., MORB-like forearc basalts) can form by decompression melting of the upwelling asthenosphere at spreading centers, such as during the process of SI (Reagan et al., 2010). Thus, we propose that the interplay between S-saturated MORB-like melts (Si-undersaturated) and the reacting harzburgite led to the consumption of Opx and the formation of Ol and Cpx (Fig. 4l), and PPGE-enriched sulfides (Fig. A4).

5.6. Genesis of the Gomsiqe dunites and chromitites

5.6.1. Inferences from the major oxide compositions of the parental melts

The compositions of chromium spinels in replacive dunites and associated podifrom chromitites have been widely used to shed light on the geochemical characteristics of their parental melts and formational tectonic settings (Kamenetsky et al., 2001; Zhou et al., 2014; Zhang et al., 2019). We calculated the Al_2O_3 and TiO_2 contents and FeO/MgO ratios of the parental melts of the Gomsiqe dunites and associated disseminated chromitites (Table A4; Fig. 14a) (Wu et al., 2018). The Al_2O_3 and TiO_2 contents of the calculated parental melts of dunites and chormitites are identical to those of lavas transitional between MORB and BON (Fig. 14a) (Reagan et al., 2010). In the $(FeO/MgO)_{melt}$ vs. $(Al_2O_3)_{melt}$ plot (Fig. 14b), the compositions of the calculated parental melts of dunites and chormitites are similar to those of the Izu-Bonin forearc basalts (Reagan et al., 2010) and Mirdita MORB (Saccani et al., 2018).

On the other hand, the occurrence of primary hydrous inclusions (i.e., Na-phlogopite, pargasite) within the Gomsiqe high-Al chromium spinels (Fig. 4) imply that the trapped parental melts were enriched in Na_2O and H_2O (Zhou et al., 2014). In addition, the compositions of the pargasite inclusions within the Gomsiqe dunites and chromitites are quite similar to those within the IBM medium-Cr# dunites (Fig. 5f) (Morishita et al., 2011). The IBM medium-Cr# dunites (Cr# of 40–60) are products of the interaction between the harzburgitic mantle and MORB-like forearc basalts during initial subduction of the Pacific plate (Morishita et al., 2011).

5.6.2. Constraints from trace elements of spinels

Geochemical features of parental melts can also be estimated from trace element compositions of spinels (Page and Barnes, 2009; Zhou et al., 2014). During mantle partial melting, V and Sc show similar chemical properties (Lee et al., 2005; Su et al., 2019), V is more redox-sensitive, relative to Sc. Thus, the V/Sc ratio can be used to assess the fo_2 conditions of parental magmas (Lee et al., 2005). In Fig. 14c, from IBM forearc basalts (FAB), to IBM lavas transitional between FAB and BON, to BON, the V/Sc ratios decrease with decreasing Ti. The Mirdita volcanic rocks show a similar trend. The calculated melts in equilibrium with Gomsiqe dunites and chromitites have oxygen fugacity of their mantle source regions comparable to those of lavas transitional between FAB and BON (Fig. 14c). The large variation in the V/Sc ratios of the parental melts of Gomsiqe chromitites suggests the involvement of fluids, which modify the fo_2 of their mantle source (Lee et al., 2005; Pan et al., 2022) and can be verified by the occurrence of hydrous mineral inclusions (Fig. 4).

5.6.3. Constraints from trace elements of olivines

Given that mantle dunites represent the conduits for melt migration (Kelemen et al., 1995), the composition of olivine trace elements may impose constraints on the nature of the migrating melts (De Hoog et al., 2010; Sanfilippo et al., 2014; Wang et al., 2021). The markedly variable

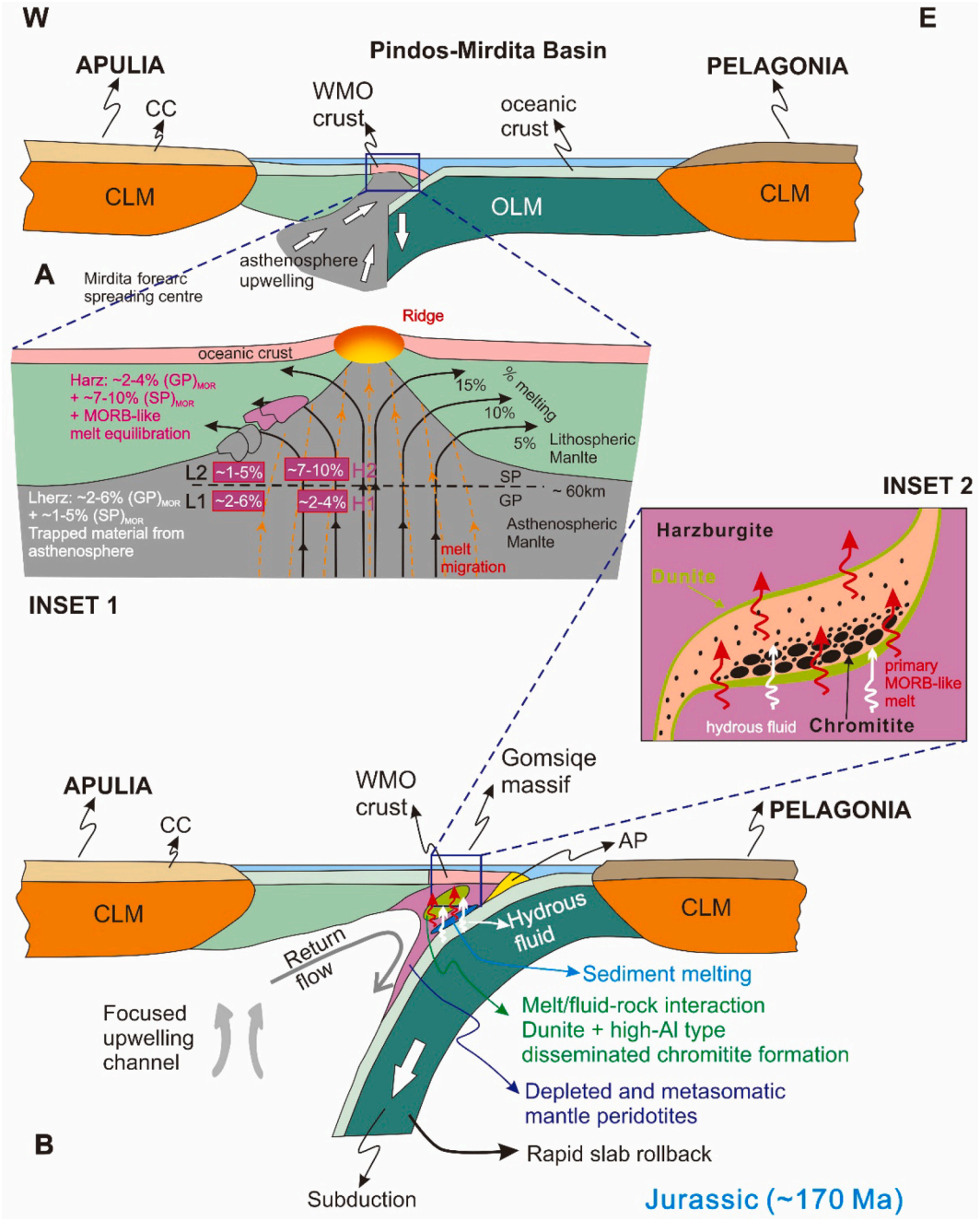

Fig. 15. Schematic formation model for a multistage evolution of the Gomsiqe massif, Mirdita ophiolite during subduction initiation. The model includes first stage grt-facies fractional melting (i.e., L1 and H1; inset 1), second stage spl-facies fractional (i.e., L2 and H2), and third stage melt equilibration with residual solids formed in the second stage. Dunite and disseminated chromitites were formed through additional reactions between new formed MORB melts and residual harzburgite formed in the second stage. Hydrous fluid derived from subducting slab also participated in these reactions (inset 2). Abbreviations: WMO-western Mirdita ophiolite; OLM-oceanic lithosphere mantle; CLM-continental lithosphere mantle; CC-continental crust; AP-accretion prism. See text for discussion.

Ti/Y values of olivines from Gomsiqe dunites and disseminated chromitites (Fig. 7c) may be the consequence of the interplay between olivine and the migrating melts enriched in incompatible elements, such as Ti, as also illustrated by the Lanzo South replacive dunites (Sanfilippo et al., 2014). Generally, the V/Sc ratios in peridotitic olivines can constrain the oxidation state during mantle melting and metasomatism (Foley et al., 2013). Gomsiqe basal lherzolites and harzburgites are characterized by high V/Sc ratios (Fig. 7), while the olivines in the dunites and disseminated chromitites show relatively lower V/Sc values. The high V/Sc ratios indicate that reducing conditions during the Neo-Tethys depletion event characterize the lherzolites and harzburgites, and the lower V/Sc ratios imply a more oxidizing environment for the dunites and chromitites (Foley et al., 2013). This result agrees with the mantle oxygen fugacity (fO_2) estimation of the basal lherzolites, harzburgites, and dunites (including the disseminated chromitites) (Fig. 13).

5.7. Links between the Gomsiqe massif formation and subduction initiation

A forearc tectonic setting followed by a subduction initiation origin has the least resistance for the formation of the Mirdita ophiolites (Saccani et al., 2018). Here, we propose that the Gomsiqe ultramafic rocks represent the archive of the early stage (i.e., the birth stage) of the SI processes. On this basis, the present study completes our

understanding of mantle-melt evolution processes in the earliest stage of subduction initiation based on our new data and the regional Tethyan geodynamic framework (Fig. 15).

The initiation of subduction can be caused by far-field forcing (i.e., induced subduction initiation) and lithospheric gravitational instability (i.e., spontaneous subduction initiation) at weak pre-existing structures (Stern et al., 2013; Stern and Bloomer, 1992), or by mantle plume (i.e., plume-induced subduction initiation; Macpherson and Hall, 2001). Subduction initiation is closely related to the early stages (e.g., birth and youth stages) of the life cycle of SSZ ophiolites (Shervais, 2001; Whattam and Stern, 2011). The birth stage is marked by asthenosphere upwelling above the sinking oceanic slab, generating MORB-like forearc basalt by decompression partial melting with a lherzolitic/harzburgitic residue (Fig. 15a). The most popular geodynamic model at this stage is the hinge rollback model (Stern and Bloomer, 1992). The rapid rollback of the sinking slab, during and after its initiation, allows continuous upwelling of the asthenosphere, which will produce new primitive melts that will interact with residual peridotites (Dilek et al., 2008; Wu et al., 2018).

Initial subduction of the Pindos-Mirdita basin occurred in response to continental collisions (i.e., the Sakarya collision) that occurred farther north on the European side of the Laurasia continent (induced subduction initiation; Dilek et al., 2008). The Pindos-Mirdita oceanic slab began to sink, inducing upwelling of the asthenosphere. In the Gomsiqe massif, the basal lherzolites represent remnants which underwent very low-degree partial melting due to adiabatic decompression melting of the rising asthenosphere mantle, without subducting slab influence. The harzburgites sustained a higher degree of partial melting during this process. Both peridotite types underwent variable grt-facies melting before spl-facies melting (Figs. 12 and 15). The harzburgites were affected by newly formed MORB-affinity melt impregnation during their extraction and migration, while the lherzolites were not affected (Fig. 11). Mantle processes forming such peridotites are similar to those observed in abyssal peridotites (Warren, 2016). According to the model of Nicolas et al. (1999), an inferred ridge axis is located east of the Gomsiqe massif (Fig. 1). We consider that this tectonic situation may have been responsible for the local presence of basal lherzolites in this area (Fig. 15).

In our model, the Mirdita ophiolite developed above a west-dipping subduction zone followed by subsequent rapid slab retreat (Fig. 15a) (Dilek et al., 2008). The return mantle flow was advanced by the eastward slab rollback. Provided that the flow of the asthenosphere is nearly horizontal, decompression-induced melting is rare. Consequently, the newly upwelling hot asthenospheric mantle may have thermally eroded the base of pre-existing oceanic lithospheric mantle (i.e., Gomsiqe basal lherzolites and harzburgites), which is recorded by the re-equilibration of the 2^+ cations (such as Ca, Fe, and Mg) between Opx and Cpx, while the 3^+ cations remained the same (Fig. 10e-f). Alternatively, such re-equilibration in the peridotites may also be related to the obduction during their finally emplacement process. As subduction continued, the newly formed MORB-like forearc basalt melts were fluxed with minor fluids derived from the subducted slab to generate lavas transitional between FAB and BON (Fig. 15) (Reagan et al., 2010). The transitional lavas migrated upward and reacted with the former formed upper mantle peridotites, producing the Gomsiqe high-Al (Cr# < 60) replacive dunite and disseminated chromitites (González-Jiménez et al., 2014; Kelemen et al., 1995; Liang et al., 2010; Xiong et al., 2017b).

6. Conclusions

In this study, we propose that the Gomsiqe massif in the western Mirdita ophiolite represents fragments of oceanic lithosphere emplaced following closure of the Pindos-Mirdita Neo-Tethys Ocean during the earliest stage (i.e., birth stage) of the subduction initiation process. The Gomsiqe peridotites (i.e., lherzolite, harzburgite, and dunite) and podiform chromitites display multidisciplinary evidence for multiple episodes (time-progressive) of partial melting, melt extraction, and melt/fluid-rock interactions at various scales. They collectively preserve high-fidelity petrogeochemical and physical responses to the earliest stage of subduction initiation, which previously has been mostly documented for crustal rocks (Saccani et al., 2018). During and after the subduction initiation process, initial steepening and subsequent rapid rollback of the slab triggered large-scale passive upwelling, which can rapidly evolve into a self-maintaining, low-viscosity channel (McGowan et al., 2015). This mechanism can allow hot upwelling asthenosphere to thermally eroding the base of the pre-existing oceanic lithospheric mantle, and can repeatedly inject primary melts to meet more evolved melts, which leads to mingling, mixing, and reacting, producing more chromites (González-Jiménez et al., 2014), and eventually, a giant chromitite ore. This subduction initiation process may also allow microdiamonds and other ultrahigh-pressure minerals to rapidly (6–10 m.y.) become excavated from the deep upper mantle into shallow mantle levels (c. 60 km), as reported in the Skenderbeu (Wu et al., 2019) and Bulqiza massifs (Xiong et al., 2017a) in the western and eastern Mirdita ophiolite, respectively. This study shows the importance of the oceanic mantle for a comprehensive understanding of the processes of subduction initiation and the processes of heat and mass transfer in the Earth's cycling system.

Supplementary data to this article can be found online at https://doi.org/10.1016/j.lithos.2022.106937.

Declaration of Competing Interest

The authors declare that they have no known competing financial interests or personal relationships that could have appeared to influence the work reported in this paper.

Acknowledgments

We thank our colleagues in CARMA, the Polytechnic University of Tirana (Albania), and the Geological Survey of Albania for their assistance with the logistics of our fieldwork in the Mirdita ophiolite. We thank Drs. Qing Xiong and Xiang Zhou for their suggestions and comments on earlier versions of the manuscript. We thank the Editor Di-Cheng Zhu, reviewer Chuan-Zhou Liu and an anonymous reviewer for their constructive reviews, which have greatly improved the manuscript. This research was supported by the National Natural Science Foundation of China (92062215, 41802055, 42102248, 41720104009, 41802034, 41703053, 41762005).

References

Abe, N., 2011. Petrology of podiform chromitite from the ocean floor at the 15. DEG. 20'N FZ in the MAR, Site 1271, ODP Leg 209. J. Mineral. Petrol. Sci. 106, 97–102.
Akizawa, N., Arai, S., Tamura, A., 2012. Behavior of MORB magmas at uppermost mantle beneath a fast-spreading axis: an example from Wadi Fizh of the northern Oman ophiolite. Contrib. Mineral. Petrol. 164, 601–625. https://doi.org/10.1007/s00410-012-0762-4.
Alabaster, T., Pearce, J.A., Malpas, J., 1982. The volcanic stratigraphy and petrogenesis of the Oman ophiolite complex. Contrib. Mineral. Petrol. 81 (3), 168–183.
Alard, O., Griffin, W.L., Lorand, J.P., Jackson, S.E., O'Reilly, S.Y., 2000. Non-chondritic distribution of the highly siderophile elements in mantle sulphides. Nature 407, 891–894.
Arai, S., 1994. Characterization of spinel peridotites by olivine-spinel compositional relationships: review and interpretation. Chem. Geol. 113, 191–204.
Arai, S., Matsukage, K., 1998. Petrology of a chromitite micropod from Hess Deep, equatorial Pacific: a comparison between abyssal and alpine-type podiform chromitites. Lithos 43, 1–14.
Ballhaus, C., Berry, R.F., Green, D.H., 1991. High-pressure experimental calibration of the olivine-orthopyroxene-spinel oxygen geobarometer: implications for the oxidation state of the upper mantle. Contrib. Mineral. Petrol. 107, 27–40.
Barnes, S.J., Roeder, P.L., 2001. The range of spinel compositions in terrestrial mafic and ultramafic rocks. J. Petrol. 42, 2279–2302, 10.1093/petrology/42.12.2279.
Beard, A.D., Downes, H., Mason, P.R.D., Vetrin, V.R., 2007. Depletion and enrichment processes in the lithospheric mantle beneath the Kola Peninsula (Russia): evidence from spinel lherzolite and wehrlite xenoliths. Lithos 94, 1–24. https://doi.org/10.1016/j.lithos.2006.02.002.

Bizimis, M., Salters, V.J.M., Bonatti, E., 2000. Trace and REE content of clinopyroxenes from supra-subduction zone peridotites. Implications for melting and enrichment processes in island arcs. Chem. Geol. 165, 67–85.
Brey, G.P., Kohler, T., 1990. Geothermobarometry in Four-phase Lherzolites II. New Thermobarometers, and Practical Assessment of existing Thermobarometers. J. Petrol. 31, 1353–1378. https://doi.org/10.1093/petrology/31.6.1353.
Dare, S.A.S., Pearce, J.A., McDonald, I., Styles, M.T., 2009. Tectonic discrimination of peridotites using fO 2–Cr# and Ga–Ti–Fe III systematics in chrome–spinel. Chem. Geol. 261, 199–216.
De Hoog, J.C.M., Gall, L., Cornell, D.H., 2010. Trace-element geochemistry of mantle olivine and application to mantle petrogenesis and geothermobarometry. Chem. Geol. 270, 196–215. https://doi.org/10.1016/j.chemgeo.2009.11.017.
Dilek, Y., 2003. Ophiolite concept and its evolution. Special Papers-Geol. Soc. Am. 373, 1–16.
Dilek, Y., Furnes, H., Shallo, M., 2008. Geochemistry of the Jurassic Mirdita Ophiolite (Albania) and the MORB to SSZ evolution of a marginal basin oceanic crust. Lithos 100, 174–209.
Foley, S.F., Prelevic, D., Rehfeldt, T., Jacob, D.E., 2013. Minor and trace elements in olivines as probes into early igneous and mantle melting processes. Earth Planet. Sci. Lett. 363, 181–191. https://doi.org/10.1016/j.epsl.2012.11.025.
Gale, A., Dalton, C.A., Langmuir, C.H., Su, Y.J., Schilling, J.G., 2013. The mean composition of ocean ridge basalts. Geochem. Geophys. Geosyst. 14, 489–518.
González-Jiménez, J.M., Griffin, W.L., Proenza, J.A., Gervilla, F., O'Reilly, S.Y., Akbulut, M., Pearson, N.J., Arai, S., 2014. Chromitites in ophiolites: how, where, when, why? Part II. The crystallization of chromitites. Lithos 189, 140–158.
Hanghøj, K., Kelemen, P.B., Hassler, D., Godard, M., 2010. Composition and genesis of depleted mantle peridotites from the Wadi Tayin Massif, Oman Ophiolite; major and trace element geochemistry, and Os isotope and PGE systematics. J. Petrol. 51, 201–227. https://doi.org/10.1093/petrology/egp077.
He, Y., Zhu, X., She, Y., Ma, J., Sun, J., Gao, Z., Wan, H., Chen, Y., 2021. Mechanism of formation of podiform chromitite: Insights from the oxidation states of podiform chromitites and host peridotites from the Luobusa ophiolite, southern Tibet. Ore Geol. Rev. 139, 104483.
Hellebrand, E., Snow, J.E., Hoppe, P., Hofmann, A.W., 2002. Garnet-field melting and late-stage refertilization in 'residual' abyssal peridotites from the Central Indian Ridge. J. Petrol. 43, 2305–2338.
Herzberg, C., Condie, K., Korenaga, J., 2010. Thermal history of the Earth and its petrological expression. Earth Planet. Sci. Lett. 292 (1–2), 79–88.
Hoeck, V., Koller, F., Meisel, T., Onuzi, K., Kneringer, E., 2002. The Jurassic South Albanian ophiolites: MOR- vs. SSZ-type ophiolites. Lithos 65, 143–164.
Ishii, T., Robinson, P.T., Maekawa, H., Fiske, R., 1992. Petrological studies of peridotites from diapiric serpentinite seamounts in the Izu-Ogasawara-Mariana forearc, Leg 125. Proc. Ocean Drill. Prog. Sci. Res. 125, 445–485.
Ishizuka, O., Tani, K., Reagan, M.K., 2014. Izu-Bonin-Mariana Forearc Crust as a Modern Ophiolite Analogue. Elements 10, 115–120. https://doi.org/10.2113/gselements.10.2.115.
Johnson, K.T.M., Dick, H.J.B., Shimizu, N., 1990. Melting in the oceanic upper mantle: an ion microprobe study of diopsides in abyssal peridotites. J. Geophys. Res. Solid Earth 95, 2661–2678.
Kamenetsky, V.S., Crawford, A.J., Meffre, S., 2001. Factors controlling chemistry of magmatic spinel: an empirical study of associated olivine, Cr-spinel and melt inclusions from primitive rocks. J. Petrol. 42, 655–671.
Kelemen, P.B., Shimizu, N., Salters, V., 1995. Extraction of mid-ocean-ridge basalt from the upwelling mantle by focused flow of melt in dunite channels. Nature 375, 747–753.
Khedr, M.Z., Arai, S., Python, M., Tamura, A., 2014. Chemical variations of abyssal peridotites in the Central Oman ophiolite: evidence of oceanic mantle heterogeneity. Gondwana Res. 25, 1242–1262. https://doi.org/10.1016/j.gr.2013.05.010.
Lee, C.A., Leeman, W.P., Canil, D., Zhengxue, A.L.I., 2005. Similar V/Sc systematics in MORB and arc basalts: implications for the oxygen fugacities of their mantle source regions. J. Petrol. 46, 2313–2336.
Liang, Y., Schiemenz, A., Hesse, M.A., Parmentier, E.M., Hesthaven, J.S., 2010. High-porosity channels for melt migration in the mantle: top is the dunite and bottom is the harzburgite and lherzolite. Geophys. Res. Lett. 37, L15306. https://doi.org/10.1029/2010gl044162.
Liang, Y., Sun, C., Yao, L., 2013. A REE-in-two-pyroxene thermometer for mafic and ultramafic rocks. Geochim. Cosmochim. Acta 102, 246–260. https://doi.org/10.1016/j.gca.2012.10.035.
Liang, Y., Ji, Z., Liu, B., 2021. What can we learn from REE abundances in clinopyroxene and orthopyroxene in residual mantle peridotites? Contrib. Mineral. Petrol. 176, 24. https://doi.org/10.1007/s00410-021-01780-x.
Liu, T., Wu, F.-Y., Liu, C.-Z., Zhang, C., Ji, W.-B., Xu, Y., 2019. Reconsideration of Neo-Tethys evolution constrained from the nature of the Dazhuqu ophiolitic mantle, southern Tibet. Contrib. Mineral. Petrol. 174, 23. https://doi.org/10.1007/s00410-019-1557-7.
Macpherson, C.G., Hall, R., 2001. Tectonic setting of Eocene boninite magmatism in the Izu–Bonin–Mariana forearc. Earth Planet. Sci. Lett. 186, 215–230.
Maffione, M., Thieulot, C., van Hinsbergen, D.J.J., Morris, A., Plumper, O., Spakman, W., 2015. Dynamics of intra-oceanic subduction initiation: 1. Oceanic detachment fault inversion and the formation of forearc ophiolites. Geochem. Geophys. Geosyst. 16, 1753–1770.
McDade, P., Blundy, J.D., Wood, B.J., 2003a. Trace element partitioning on the Tinaquillo Lherzolite solidus at 1.5GPa. Phys. Earth Planet. Inter. 139, 129–147.
McDade, P., Blundy, J.D., Wood, B.J., 2003b. Trace element partitioning between mantle wedge peridotite and hydrous MgO-rich melt. Am. Mineral. 88, 1825–1831.
McDonough, W.F., Sun, S.S., 1995. The composition of the Earth. Chem. Geol. 120, 223–253. https://doi.org/10.1016/0009-2541(94)00140-4.
McGowan, N.M., Griffin, W.L., González-Jiménez, J.M., Belousova, E., Afonso, J.C., Shi, R., McCammon, C.A., Pearson, N.J., Reilly, O., S. Y, 2015. Tibetan chromitites: excavating the slab graveyard. Geology 43, 179–182.
Morishita, T., Maeda, J., Miyashita, S., Kumagai, H., Matsumoto, T., Dick, H.J.B., 2007. Petrology of local concentration of chromian spinel in dunite from the slow-spreading Southwest Indian Ridge. Eur. J. Mineral. 19, 871–882.
Morishita, T., Tani, K., Shukuno, H., Harigane, Y., Tamura, A., Kumagai, H., Hellebrand, E., 2011. Diversity of melt conduits in the Izu-Bonin-Mariana forearc mantle: implications for the earliest stage of arc magmatism. Geology 39, 411–414. https://doi.org/10.1130/g31706.1.
Nicolas, A., Boudier, F., Meshi, A., 1999. Slow spreading accretion and mantle denudation in the Mirdita ophiolite (Albania). J. Geophys. Res.-Solid Earth 104, 15155–15167.
Okamura, H., Arai, S., Kim, Y.-U., 2006. Petrology of forearc peridotite from the Hahajima Seamount, the Izu-Bonin arc, with special reference to chemical characteristics of chromian spinel. Mineral. Mag. 70, 15–26.
Page, P., Barnes, S.J., 2009. Using trace elements in chromites to constrain the origin of podiform chromitites in the Thetford Mines Ophiolite, Quebec, Canada. Econ. Geol. 104, 997–1018.
Pan, Q.-Q., Xiao, Y., Su, B.-X., Liu, X., Robinson, P.T., Cui, M.-M., Wang, J., Uysal, I., 2022. Fingerprinting stealth metasomatism in ophiolitic peridotites. Lithos 424-425, 106755.
Parkinson, I.J., Arculus, R.J., 1999. The redox state of subduction zones: insights from arc-peridotites. Chem. Geol. 160, 409–423.
Parkinson, I.J., Pearce, J.A., 1998. Peridotites from the Izu–Bonin–Mariana forearc (ODP Leg 125): evidence for mantle melting and melt–mantle interaction in a supra-subduction zone setting. J. Petrol. 39, 1577–1618.
Pearce, J.A., Lippard, S.J., Roberts, S., 1984. Characteristics and tectonic significance of supra-subduction zone ophiolites. Geol. Soc. Lond., Spec. Publ. 16 (1), 77–94.
Pearce, J.A., van der Laan, S.R., Arculus, R.J., Murton, B.J., Ishii, T., Peate, D.W., Parkinson, I.J., 1992. Boninite and harzburgite from Leg 125 (Bonin-Mariana forearc): a case study of magma genesis during the initial stages of subduction. Proc. Ocean Drill. Prog. Sci. Res. 125, 623–659.
Pearce, J.A., Barker, P.F., Edwards, S.J., Parkinson, I.J., Leat, P.T., 2000. Geochemistry and tectonic significance of peridotites from the South Sandwich arc–basin system, South Atlantic. Contrib. Mineral. Petrol. 139, 36–53.
Reagan, M.K., Ishizuka, O., Stern, R.J., Kelley, K.A., Ohara, Y., Blichert-Toft, J., Bloomer, S.H., Cash, J., Fryer, P., Hanan, B.B., 2010. Fore-arc basalts and subduction initiation in the Izu-Bonin- Mariana system. Geochem. Geophys. Geosyst. 11, 427–428.
Saccani, E., Dilek, Y., Photiades, A., 2018. Time-progressive mantle-melt evolution and magma production in a Tethyan marginal sea: a case study of the Albanide-Hellenide ophiolites. Lithosphere 10, 35–53.
Sanfilippo, A., Tribuzio, R., Tiepolo, M., 2014. Mantle–crust interactions in the oceanic lithosphere: constraints from minor and trace elements in olivine. Geochim. Cosmochim. Acta 141, 423–439. https://doi.org/10.1016/j.gca.2014.06.012.
Seyler, M., Toplis, M.J., Lorand, J.P., Luguet, A., Cannat, M., 2001. Clinopyroxene microtextures reveal incompletely extracted melts in abyssal peridotites. Geology 29, 155–158.
Seyler, M., Lorand, J.P., Dick, H.J.B., Drouin, M., 2007. Pervasive melt percolation reactions in ultra-depleted refractory harzburgites at the Mid-Atlantic Ridge, 15° 20′N: ODP Hole 1274A. Contrib. Mineral. Petrol. 153, 303–319. https://doi.org/10.1007/s00410-006-0148-6.
Shervais, J.W., 2001. Birth, death, and resurrection: the life cycle of suprasubduction zone ophiolites. Geochem. Geophys. Geosyst. 2, 2000GC000080.
Snow, J.E., Dick, H.J.B., 1995. Pervasive magnesium loss by marine weathering of peridotite. Geochim. Cosmochim. Acta 59, 4219–4235.
Sobolev, A.V., Hofmann, A.W., Kuzmin, D.V., Yaxley, G.M., Arndt, N.T., Chung, S.L., Danyushevsky, L.V., 2007. The amount of recycled crust in sources of mantle-derived melts. Science 316, 412–417. https://doi.org/10.1126/science.1138113.
Stern, R.J., Bloomer, S.H., 1992. Subduction zone infancy: examples from the Eocene Izu-Bonin-Mariana and Jurassic California arcs. Geol. Soc. Am. Bull. 104, 1621–1636. https://doi.org/10.1130/0016-7606(1992)104<1621:Szieft>2.3.Co;2.
Stern, R.J., Reagan, M., Ishizuka, O., Ohara, Y., Whattam, S., 2013. To understand subduction initiation, study forearc crust: to understand forearc crust, study ophiolites. Lithoshere 4, 469–483.
Su, B., Zhou, M., Jing, J., Robinson, P.T., Chen, C., Xiao, Y., Liu, X., Shi, R., Lenaz, D., Hu, Y., 2019. Distinctive melt activity and chromite mineralization in Luobusa and Purang ophiolites, southern Tibet: constraints from trace element compositions of chromite and olivine. Sci. Bull. 64 (2), 108–121.
Su, B.-X., Robinson, P.T., Chen, C., Xiao, Y., Melcher, F., Bai, Y., Gu, X.-Y., Uysal, I., Lenaz, D., 2020. The occurrence, origin, and fate of water in chromitites in ophiolites. Am. Mineral. 105 (6), 894–903.
Sun, C., Liang, Y., 2012. Distribution of REE between clinopyroxene and basaltic melt along a mantle adiabat: effects of major element composition, water, and temperature. Contrib. Mineral. Petrol. 163, 807–823.
Takazawa, E., Okayasu, T., Satoh, K., 2003. Geochemistry and origin of the basal lherzolites from the northern Oman ophiolite (northern Fizh block). Geochem. Geophys. Geosyst. 4, 34.
Wang, J., Su, B.-X., Robinson, P.T., Xiao, Y., Bai, Y., Liu, X., Sakyi, P.A., Jing, J.-J., Chen, C., Liang, Z., Bao, Z.-A., 2021. Trace elements in olivine: Proxies for petrogenesis, mineralization and discrimination of mafic-ultramafic rocks. Lithos 388-389, 106085.

Warren, J.M., 2016. Global variations in abyssal peridotite compositions. Lithos 248-251, 193–219.
Whattam, S.A., Stern, R.J., 2011. The 'subduction initiation rule': a key for linking ophiolites, intra-oceanic forearcs, and subduction initiation. Contrib. Mineral. Petrol. 162, 1031–1045.
Witt-Eickschen, G., O'Neill, H.S.C., 2005. The effect of temperature on the equilibrium distribution of trace elements between clinopyroxene, orthopyroxene, olivine and spinel in upper mantle peridotite. Chem. Geol. 221, 65–101. https://doi.org/10.1016/j.chemgeo.2005.04.005.
Witt-Eickschen, G., Seck, H.A., 1991. Solubility of Ca and Al in orthopyroxene from spinel peridotite: an improved version of an empirical geothermometer. Contrib. Mineral. Petrol. 106, 431–439.
Woodland, S.J., Pearson, D.G., Thirlwall, M.F., 2002. A platinum group element and Re–Os isotope investigation of siderophile element recycling in subduction zones: comparison of grenada, lesser antilles Arc, and the Izu–Bonin Arc. J. Petrol. 43, 171–198.
Workman, R.K., Hart, S.R., 2005. Major and trace element composition of the depleted MORB mantle (DMM). Earth Planet. Sci. Lett. 231, 53–72.
Wu, W., Yang, J., Dilek, Y., Milushi, I., Lian, D., 2018. Multiple episodes of melting, depletion, and enrichment of the Tethyan mantle: petrogenesis of the peridotites and chromitites in the Jurassic Skenderbeu massif, Mirdita ophiolite, Albania. Lithosphere 10, 54–78.
Wu, W., Yang, J., Wirth, R., Zheng, J., Lian, D., Qiu, T., Milushi, I., 2019. Carbon and nitrogen isotopes and mineral inclusions in diamonds from chromitites of the Mirdita ophiolite (Albania) demonstrate recycling of oceanic crust into the mantle. Am. Mineral. 104, 485–500. https://doi.org/10.2138/am-2019-6751.
Xhomo, A., Kodra, A., Dimo, L.L., Xhafa, Z., Nazaj, S.H., Nakuci, V., Yzeiraj, D., Lula, F., Sadushi, P., Shallo, M., Vranaj, A., Melo, V., 2002. Geological Map of Albania: Albanian Geological Survey, scale 1:200,000.
Xiong, F., Yang, J., Robinson, P.T., Dilek, Y., Milushi, I., Xu, X., Zhou, W., Zhang, Z., Rong, H., 2017a. Diamonds discovered from high–Cr podiform chromitites of Bulqiza, Eastern Mirdita Ophiolite, Albania. Acta Geol. Sinica (English Edition) 91, 455–468.
Xiong, Q., Griffin, W.L., Zheng, J.P., Pearson, N.J., O'Reilly, S.Y., 2017b. Two-layered oceanic lithospheric mantle in a Tibetan ophiolite produced by episodic subduction of Tethyan slabs. Geochem. Geophys. Geosyst. 18, 1189–1213.
Zhang, P.-F., Zhou, M.-F., Robinson, P.T., Pearce, J.A., Malpas, J., Liu, Q.-Y., Xia, X.-P., 2019. Evolution of nascent mantle wedges during subduction initiation: Li-O isotopic evidence from the Luobusa ophiolite, Tibet. Geochim. Cosmochim. Acta 245, 35–58. https://doi.org/10.1016/j.gca.2018.09.037.
Zhou, M.-F., Robinson, P.T., Su, B.-X., Gao, J.-F., Li, J.-W., Yang, J.-S., Malpas, J., 2014. Compositions of chromite, associated minerals, and parental magmas of podiform chromite deposits: the role of slab contamination of asthenospheric melts in suprasubduction zone environments. Gondwana Res. 26, 262–283.